Chapter 4

Aeromagnetic and Marine Measurements

Mohamed Hamoudi, Yoann Quesnel, Jérôme Dyment, and Vincent Lesur

Abstract Modern magnetic measurements have been acquired since the 1940s over land and the 1950s over oceans. Such measurements are collected using magnetometer sensors rigidly fixed to the airframe or towed in a bird for airborne or in a fish in marine surveys using a cable long enough to avoid the ship/airplane magnetic effect. Positioning problems have been considerably reduced by the Global Positioning System (GPS). Considerable progress has been made in geomagnetic instrumentation increasing the accuracy from ∼10 nT or better in the 1960s to ∼0.1 nT or more nowadays. Scalar magnetometers, less sensitive to orientation problems than the fluxgate vector instruments, are the most commnonly used for total-field intensity measurement. Optical pumping alkali vapor magnetometers with high sampling rate and high sensitivity are generally used aboard airframes whereas proton precession magnetometers (including Overhauser) are favored at sea. Scalar magnetic anomalies are calculated by subtraction of global core field models like the International Geomagnetic Reference Field (IGRF) after subtraction of an external magnetic field estimate using magnetic observatories or temporary magnetic stations. The external field correction using an auxiliary station is often not possible in marine measurements. However comprehensive models such as CM4 can be used to provide adequate core and external magnetic fields, particularly for almost all early magnetic measurements which were not corrected for the external field. In the case of airborne measurements such global models help to define a reference level for global mapping of the anomaly field. The current marine dataset adequately covers most of the Northern Hemisphere oceanic areas while major gaps are observed in the southern Indian and Pacific oceans. Airborne measurements cover all the world, except oceanic areas and large part of Antarctica. Data are however often not available when owned by private companies. The data released are mainly owned by governmental agencies. The derived airborne/marine magnetic anomaly maps combined with long-wavelength satellite maps help scientists to better understand the structure and the evolution of the lithosphere at local, regional and global scales. Marine magnetic observations are also made at depth, near the seafloor, in order to access shorter wavelengths of the magnetic field for high resolution studies. Airborne High Resolution Anomaly Maps (HRAM) are also nowadays the new trends pushing towards the generalisation of the Unmanned Aerial Vehicles (UAV) or Autonomous Underwater Vehicles (AUV) or Remotely Operated Vehicles (ROV) magnetic surveys.

4.1 General Introduction

It has been known for some two thousand years that pieces of magnetized rocks attract (or repel) each other. However Gilbert's statement in the very beginning of the 17th century – that the Earth behaves itself as a great magnet – is a milestone in Earth's magnetism. Latter on, by the mid-19th century, it has been realized that magnetic instruments (e.g., magnetic theodolite), normally operated for measuring the Earth's magnetic field variations, might be employed to discover magnetic ore bodies (Telford et al. 1990).

M. Hamoudi (✉)
Helmholtz Centre Potsdam, GFZ German Research Centre for Geosciences, Telegrafenberg, F 407, 14473, Potsdam, Germany
e-mail: hamoudi@gfz-postdam.de

M. Mandea, M. Korte (eds.), *Geomagnetic Observations and Models*, IAGA Special Sopron Book Series 5,
DOI 10.1007/978-90-481-9858-0_4,

Advances in building magnetic instrumentations have been very rapid since World War II with the first Magnetic Airborne Detector (MAD) designed for submarines and mines detection. From the early 1950s, not only geological national agencies but also oil and mining companies have shown a great interest for aeromagnetic and marine surveys.

It is worth to mention that the marine magnetic data acquired during the 1950s and early 1960s have played an important role in uncovering plate tectonics, starting a revolution in geosciences. As a consequence, the systematic acquisition of marine magnetic data helped to decipher the age of ocean crusts and carry out paleogeographic reconstructions. This has led to a first order picture of the Earth's lithosphere evolution for the last 200 millions years. Moreover, advancement in magnetic instrumentations as well as positioning systems have allowed, on one hand to achieve the required precision for the global satellite mapping, and on the other hand to derive high-resolution magnetic mapping at low altitude both at sea and on land. Geological mapping has directly benefitted from the available airborne and marine magnetic surveys. However, more efforts are needed for a full coverage of the Earth's surface with magnetic survey data.

This manuscript is intended to give a non exhaustive review of the progress in aeromagnetic and marine magnetic surveys over more than half of century. Let us note that the paper is built around two distinct parts: the first one is devoted to aeromagnetic surveys and the second to marine magnetics. Even if the progress and evolution of both fields are closely related, they are described separately in order to better emphasize their specificities.

4.2 Introduction to Aeromagnetics

The main or global magnetic field of the Earth is generated in the conducting fluid outer core by geodynamo processes (Braginski and Roberts 1995). This field is much stronger than the field generated in the Earth's lithosphere. During magnetic surveys, numerous sources of the magnetic field contribute to the measured signal, but the main target is the field generated in the magnetized rocks.

Potential field exploration methods, like gravity and magnetism, are considered as passive methods (Heiland 1929, 1940) because the measured signal is the response permanently generated by physical property contrasts in the rocks. These gravity or magnetic responses may be measured remotely, without having direct access to the rocks. The physical contrasts considered are either density contrasts for gravity, or remnant and induced magnetization contrasts for magnetism. We have known since Newton that all rocks contribute to the observed gravity field, but only magnetized rocks generate a magnetic field. Geological formations may be very strongly or very weakly magnetized, depending on their magnetite (or any iron or sulphide oxide) content (Heiland 1940). Unlike density, magnetization is strongly temperature dependent (Kitte 2005) and exists only if this temperature does not exceed a certain temperature-threshold called the Curie temperature. This Curie temperature varies between 300°C and 1200°C for iron sulphides or oxides (Frost and Shive 1986), and is approximately 580°C for magnetite at atmospheric pressure (Blakely 1988). Above the Curie temperature, spontaneous magnetization vanishes, and minerals exhibit paramagnetic susceptibility that has a small effect compared to magnetization (Kittel 2005). Therefore rocks are essentially non-magnetic at temperatures greater than the Curie temperature of the most important magnetic mineral in the rocks. Taking into account a normal geothermal gradient, sources of the measured magnetic signal are then restricted to 30–40 km depth, except in old cratonic areas where the Curie depth at which the temperature reaches the Curie temperature – may be greater (Hamoudi et al. 1998).

The success of the magnetic method and its wide spread use are due to the numerous discoveries of iron ore deposits since the mid-19th century, all around the world, in USA, Canada, (Heiland 1929, 1940), in Russia (Logachev 1947), and even before in Sweden in northern Europe (Sundberg and Lundberg 1932, Heiland 1940). The surveys were initially ground based. The depth of an ore body, assuming it can be represented as a line of poles, may be determined using the vertical gradient of the vertical field component by differencing the field at different height levels. Experiments were first proposed at the end of 19th century to measure the field at different levels in a mine and at different depths of a shaft (Heiland 1940). For ore bodies with a large depth extent, measuring the field at the Earth's surface and on a platform a few meters above was proposed. However Eve and Keys

(1933) rapidly reached the limit of the method and it became apparent that because platforms failed to give sufficient changes in the distance to the source, geophysicists were going to have to "take to the air" (Heiland 1940). Captive balloons have been used above the Kiruna ore body (Sundberg and Lundberg 1932, Heiland 1940). It was soon established that measurements in airplanes by an automatic recording device had many benefits among them great speed of survey, applicability to inaccessible areas, and "direct depth determination" (Heiland 1935, 1940, Logachev 1947).

Airborne geophysical methods have grown since their inception in the 1930s. Submarine and mine detection during World War II gave an impetus to improvements in apparatus and methods for aeromagnetic surveys (Wyckoff 1948). Since then, continuous improvements in instrumentation and positioning systems have made the aeromagnetic survey a powerful tool in multi-scale exploration. Nowadays magnetometry, spectrometry or radiometry, electromagnetic and gravity surveys are concurrently, or separately, conducted onboard moving platforms. These methods were developed beside other important geophysical methods for mineral and oil exploration. In the following, only airborne magnetic surveys will be discussed in detail. For a long time, the most distinguishing features of the aeromagnetic method, in comparison with other geophysical prospecting methods, were its low cost and its data acquisition speed (Heiland 1940; Reford and Sumner 1964) especially when compared to seismic campaigns in oil exploration. The availability of the Global Positioning System (GPS) by the early 1990s, particularly in its differential form, together with the very high sensitivity and accuracy of the magnetometers, dramatically reduced the error budget in aeromagnetic surveys. Subtle magnetic variations can now be resolved (Millegan 2005; Nabighian et al. 2005) and high-resolution aeromagnetic surveys (HRAM) are industry standard. These achievements have pushed toward "lower and lower" altitude and "higher and higher" resolution. Safety is now a crucial issue, pilots and geophysicists already having paid a heavy price with 21 crashes and 48 fatalities between 1977 and 2001 (Urquhart 2003). Advances in miniaturized electronics, GPS technology, and sensors (magnetometers, video cameras) coupled with sophisticated guidance, navigation and control systems enable the development of small Unmanned Aerial Vehicles (UAVs) for survey missions operating for extended periods of time over large geographical areas (Lum et al. 2005, Lum 2009). However, to bridge the gap between long wavelengths, say larger than 600 *km*, resolved by near-Earth orbiting satellite measurements and short wavelengths of less than about 200 km, resolved by aeromagnetic data, measurements of the magnetic field aboard stratospheric balloon flying at 30−40 km altitude prove to be also useful (Cohen et al. 1986; Achache et al. 1991; Tsvetkov et al. 1995; Nazarova et al. 2005; Tohyama et al. 2007). Most aeromagnetic data processing procedures are now fairly standard even though some minor differences still exist in leveling and gridding. There is not yet any standard format for the magnetic data as in seismic industry with the SEG-format (Paterson and Reeves 1985). Important efforts in archiving data for future use, particularly raw unfiltered data, have still to be made either by national agencies or by private companies. The best examples of problems that may arise from non-standard data archiving are given by the compilation of the 29 available aeromagnetic datasets used for the World Digital Magnetic Anomaly Map (WDMAM) project (Korhonen et al. 2007). This compiled magnetic anomaly map, containing all available wavelengths, is very useful for geological and tectonic mapping of the crust. However, the quality of each dataset covering a specific region has been hard to estimate as very few compilations have complete metadata information (Hamoudi et al. 2007). When available, metadata show compilations to be in different coordinate systems and projections. All compilations resulted from the stitching together of smaller surveys carried out at various altitudes in which the individual panels were, or were not, upward continued to a common altitude. Often, this information is provided but in general the mean altitude, or the mean terrain clearance with respect to mean sea level, is not systematically known. Panels inside each individual compilation were derived for different epochs using for the reference field either local polynomials or global models. In most cases, it was difficult to find out which model had been used to reduce the data. Because the quality of these global models is continuously improving, keeping track of the reference field used to derive the anomaly field is fundamental. Despite continuous technological developments in surveying techniques, progress in geophysical and geological interpretation of potential field data, especially the magnetic field, are

slow. It is only recently that the relationships between magnetite and geologic processes have been deeply studied (Reynolds and Schlinger 1990; Reynolds et al. 1990; Frost Shive 1986; Grant 1985a, b).

In the following sections, we present some general aspects of aeromagnetic measurements. The progress of magnetic instrumentation, aircrafts and aeronautical techniques from the 1930s pioneering era to nowadays are described in the first part. The second part concerns data acquisition from the first step of survey design to the final one of mapping the crustal magnetic field. Geological and geophysical interpretation of the aeromagnetic data is beyond the scope of the present paper.

4.3 History of Aeromagnetics

The magnetic exploration method is one of the oldest geophysical methods. It is directly tied to knowledge of terrestrial magnetism. This method was applied as early as in the mid 17th century for the location of ore bodies (Heiland 1940) and especially iron-bearing formations (Heiland 1929). The attraction of compass needles to these latter formations led to extensive use of magnetic compass as a prospecting tool in many countries, among them, Sweden, Finland, Russia, and the USA during the 19th and beginning of 20th centuries (Heiland 1929; Nabighian et al. 2005). Adolph Schmidt developed the first terrain suitable device for measurement of magnetic anomalies of geological structures in the 1920s (Heiland 1929). These magnetometers were also based on a magnetic needle system. They were used for relative measurements of Z and H (vertical and horizontal resp.) magnetic components with an uncertainty of ± 2 nT. They were used in mineral as well as oil exploration. The Earth inductor inclinator magnetometer also called the Earth inductor (Heiland 1940), was the first instrument not based on needles and which could measure both the inclination and various components of the Earth's magnetic field by the voltage induced in rotating coil (Heiland 1940; Nabighian et al. 2005).

The first recorded attempt to measure the magnetic field onboard an airframe seems to be that of Edelmann who designed in 1910 a vertical balance to be used in a balloon (Heiland 1935). Hans Lundberg, using a captive balloon above Kiruna's ore body (Sweden) in 1921, realised the first airborne magnetic measurements (Eve 1932). Pioneering aircraft surveys in 1936 and 1937 were also reported by Logachev in the former Soviet Union. The magnetometer he developed and used was an induction coil designed for measurement of the vertical component of the Earth's magnetic field. The 1936 flight test at 1000 m and 300 m altitude along a 60 km length line using an open-cockpit aircraft was above a weak ($-230, +1430$ nT) but known magnetic anomaly. The measurements obtained along 3 flight lines were compared to ground data using Schmidt's balance. They showed clearly the same anomaly although with a shift in the maximum location between the three lines. Logachev attributed this shift to errors in orientation and the divergence in values of the anomaly was ascribed to instrumental errors. His first magnetometer had about 1000 nT accuracy and 72 kg weight. The unit used at that time was the gamma (1gamma $= 1$ nT $= 10^{-9}$ T). The second airborne experiment took place in 1937. It was conducted over a strong – of the order of 30000 gammas – magnetic anomaly. Six flight lines, 30 km long, were realised with an altitude of either 200 m or 300 m (Logachev 1947) depending on the weather conditions. The main result was to prove the feasibility of magnetic surveys from an airplane. The second version of his magnetometer was only 30 kg weight and a better accuracy and accuracy of about 100 nT. The third and probably most important aeromagnetic survey reported at that time was above one of the largest ore deposits in the world – The Kursk ore body – and highest related magnetic field anomaly (Logachev 1947). The main goal of the experiment was to determine whether the depths of the upper and lower limits of the Kursk ferrous quartzites could be computed from aeromagnetic data (Logachev 1947). A total of 22 traverses (lines) were flown at an altitude between 500 and 1600 m, among them four lines laid out approximately at right angles to the strike of the geological structures. Heiland (1935) also described such experiments using an Earth's magnetic inductor. He also reported advantageous aspects of magnetic surveys from the air (Heiland 1935).

World War II certainly favoured technology developments, starting from the early 1940s. The main goal was then submarine and mine detection. Victor Vacquier with the Gulf Research & Development Company investigated in 1940 and 1941 the properties of iron-cored devices as a sensitive element of a magnetometer. He then helped developing the

magnetometer (Vacquier 1946; Wyckoff 1948; Reford and Sumner 1964, Hanna 1990). The instrument, also known as a fluxgate sensor, was suitable for airborne magnetic prospecting and could measure very weak fields of about 1 nT. This instrument was the base of the MAD (Marine Airborne Detector) heavily used for military purposes. The comprehensive history of the development of the airborne magnetometer based on fluxgate sensors can be found in Muffly (1946), Reford and Sumner (1964) and in Hanna (1990). Gulf research & Development Company in 1946 made modifications to the magnetometer for geophysical exploration. The USGS (United States Geological Survey) was also involved in airborne magnetometer developments in late 1942 (Hanna 1990). Aeroservice Corporation made a successful test flight in April 1944. Three traverses were flown at different altitudes along a line over an area in Pennsylvania (USA) where the USGS had previously made a ground survey (Hanna 1990). Different tests were also conducted in various environments (wood, swamp land) with single engine aircraft.

The need for more powerful aircraft soon became apparent during these test-flights and the use of cooperatively USGS-US Navy twin-engine aeroplanes allowed more extensive oil prospecting aeromagnetic surveys prior to the security classification restrictions being lifted in 1946 (Hanna 1990). A large number of manuscripts announcing the arrival of aeromagnetic techniques were then published. The first offshore aeromagnetic survey was conducted in 1946 over the coastal gulf of Mexico by Balsley (1946). Also more than 16,000 line kilometres of magnetic data were collected in 1944 over the northernmost part of Alaska (Hildenbrand and Raines 1990). Composite magnetic anomaly maps of the conterminous US were published in 1982 (Sexton et al. 1982). The first aeromagnetic anomaly map of the former Soviet Union and its adjacent areas was published in 1979 (Zonenshain et al. 1991). For this, an instrument with an accuracy of 2 nT labelled AM-13 (Reford and Sumner 1964; Zonenshain et al. 1991) was developed. It was based on a saturable core. In 1947 the Canadian Federal government initiated systematic national aeromagnetic surveys as an aid to both geological mapping and mineral prospecting. The Geological Survey of Canada was using a modified war surplus two-axis fluxgate magnetometer (AN/ASQ-1) acquired from the U.S. Navy. The aeromagnetic map sheet was published in 1949 at various scales (Hood 1990; 2007). More than 9,500 aeromagnetic anomaly maps of Canada and adjacent areas have been published between 1949 and 1990. This amounts to more than 9,650,000 line kilometres (Hood 1990; 2007). The first national aeromagnetic map of Canada was published in 1967 (Nabighian et al. 2005). Starting from 1969, during 22 years, the Canadian International Development Agency (CIDA) funded surveys that were carried out in more than ten countries in Africa among them Botswana, Burkina Faso, and Zimbabwe. CIDA funded also the survey in Brazil in South America, and in Pakistan (Hood 2007). The aeromagnetic method was adopted by Australia. There, the first aeromagnetic survey was flown in 1947 (Doyle 1987; Horsfall 1997). Systematic national airborne geophysical surveys by the Bureau of Mineral Resources in Australia took place in 1951 (Tarlowski et al. 1992; Horsfall 1997). More than 4,000,000 line kilometres were flown with a reconnaissance survey altitude of 150 m above ground at line spacings between 1.5 and 3.2 km. The first aeromagnetic anomaly map of Australia was published in 1976 (Tarlowski et al. 1992, 1996). The fourth edition has recently been released (Milligan and Franklin 2004) using more than 10,000,000 line kilometres. Many countries among them Finland, the former Soviet Union, and South Africa (Hildenbrand T.G. and Raines 1990; Hood 2007) have also established cost effective national airborne geophysics programs. The systematic national aeromagnetic survey of Finland started in 1951 (Korhonen 2005, Nabighian et al. 2005). The high altitude survey, around 150 m, was completed in 1972 and a new one was then started, at low altitude in the range 30–40 m and with 200 m line spacing. The first Finnish national aeromagnetic anomaly map was published in 1980 (Nabighian et al. 2005, Airo 2002). The aeromagnetic anomaly map of the Fennoscandian shield was released later on (Korhonen et al. 1999).

The history of aeromagnetic methods and their evolution is closely related to the technology evolution. Indeed, the technology has progressively evolved and the capabilities of the initial electronic equipment, at the beginning rudimentary by today's standards, developed all the while. The fluxgate magnetometer was widely used in aeromagnetic surveys until mid-1960s. Its major disadvantage for the airborne applications is that it must be oriented. It has been supplanted by proton precession magnetometers that

were introduced in the mid-1950s (Germain-Jones 1957; Nabighian et al. 2005, Hood 2007). The proton precession magnetometer is a scalar magnetometer and hence does not require any precise orientation (Reford 1980; Hood 2007). Furthermore it is very easy to operate and maintain. Its main limitation comes from its discontinuous operating mode, related to the proton's polarization (Nabighian et al. 2005). The Overhauser variant of the proton precession magnetometer uses Radio Frequency (RF) excitation that allows continuous oscillations and thereby alleviates the sampling rate problem (Nabighian et al. 2005). It is also widely used for marine surveys. Notice that the fluxgate and Overhauser magnetometers are also commonly used onboard Earth orbiting magnetic satellites like the Danish Oersted satellite (Nielsen et al. 1995), the German flight mission CHAMP (Reigber et al. 2002) and planetary missions like the Lunar (Binder 1998; Hood et al. 2001) or the Martian (Acuña et al. 1999) missions. In 1957, almost at the same time as proton precession magnetometers became available, optically pumped alkali vapour magnetometers were introduced. The first instrument was used in airborne surveys in 1962 (Reford 1980; Jensen 1965). Three types of instruments were developed by different companies and are based on different alkali gases: Rubidium or Cesium, Potassium or Helium (Jensen 1965). Today, these optically pumped alkali vapour magnetometers are the most often used instruments in magnetic surveys for airborne, shipborne or ground exploration (Nabighian et al. 2005). It is worth mentioning that these magnetometers have excellent sensitivity, nowadays of the order of $1\text{pT}(\sqrt{\text{Hz}})^1 (1\text{pT} = 10^{-3}\ \text{nT} = 10^{-12}\ \text{T})$, and a very high sampling rate e.g., 10 Hz is common. Although the gradiometer mode was experimented with in the 1960s (Hood 2007), it was only in the early seventies that measuring the horizontal and vertical magnetic gradients was recognized as very important for enhancing near surface magnetic sources and for reducing noise level (Paterson and Reeves 1985). The advantage of a measured vertical gradient over a calculated one has long been debated (Grant 1972; Doll et al. 2006). The former is the difference in magnetic intensity between two sensors and the latter is derived using gridded total field maps using Fourier analysis or other method (Grant 1970). The first experiments using two sensors in which one sensor is fixed and the second being towed in a bird some tens of meters below started in the 1960s for petroleum exploration (Paterson and Reeves 1985). Even though the measurements were made with high accuracy using an optically pumped Rubidium sensor (Slack et al. 1967), the results were not convincingly superior to the computed gradient. A system for measuring the vertical gradient using rubidium-vapour sensors rigidly mounted in a twin boom was soon adopted by Geological Survey of Canada (Hood 2007). The separation between the sensors was 1.83 m (6 ft). This is not very useful for petroleum exploration but well adapted for mineral surveys (Hood et al. 1976). The gradiometers have been improved both for vertical, with separation of 0.5 or 1 m, and horizontal, with separation of 1 or 1.7 m, measurements and have been used in many high-resolution applications (Doll et al. 2006). The next generation of magnetometers that will quantitatively enhance the accuracy of mapping, are cryogenic magnetometers based on the electrical superconducting property of conducting material in low temperature liquid-helium (Zimmerman and Campbell 1975, Stolz et al. 2006). The acronym of this magnetometer is SQUID, standing for Superconducting Quantum Interference Device. Until recently the main limitation on the extensive use of SQUID magnetometer for airborne purposes came from the constraint related to liquid Helium maintenance (Stolz, 2006). A prototype was designed in 1997 and a portable version was operated as a full tensor gradiometer (three components of the gradient in each direction of the Cartesian coordinate system of the field) in 2003. The very sensitive sensor (a few femto Tesla) is towed from a helicopter and is suspended on a long cable to eliminate noise from the aircraft. This system was commissioned in 2008 and airborne geophysical surveys are being conducted by private companies (Exploration Trends & Development in 2008).

The onboard recording data system is an important part of the airborne geophysical survey. Analogue recording was a limiting factor in data acquisition and hence in the quality of surveys. In multi-channel data acquisition, the digital data recording associated with high storage capacity and the ability to verify and store unlimited quantity of aeronautical and geophysical parameters during the flight surveys, greatly improved the quality of surveys. The high sampling rates of magnetic readings and the accuracy of measurement are now easily handled and high-resolution mapping is achieved (Paterson and Reeves 1985).

Aeronautical evolution together with positioning and attitude system improvements significantly contributed to the progresses made in aeromagnetic survey accuracy, especially over oceanic areas where the positioning issue is crucial. Indeed, the snapshot photographic technique developed in 1952 by Jensen over land had an accuracy of 50 m. The flight path recovery is derived by extrapolation between points. Loran-C (Decca system) Radio positioning was then used over land and offshore, the accuracy achieved offshore was ≈500 m (Hofmann-Wellenhof et al. 2003; Urquhart 2003). The Doppler radar that provides a positioning accuracy around 5 and 10 m along tracks later replaced this system. Then the Inertial Navigation System was introduced, giving 5–10 m relative lateral position accuracy along track. The Mini-Ranger radio systems when used allowed 2 m accuracy over 75 km range (direct line of sight). The best positioning system since the 1980s is the satellite based GPS. The first use of GPS for detailed offshore aeromagnetic survey was made in 1985 (Hood 2007). The position accuracy of an aircraft with a single receiver is of the order of 20 m in the horizontal plane and much larger for the height (2–3 times horizontal error). The differential GPS mode (dGPS) allows much higher accuracy, of the order of a fraction of a centimetre in the carrier phase dGPS. Laser altimeters, now currently used in detailed or high-resolution surveys, provide centimetre precision altitude (Exploration trends & Development in 2008). This very high accuracy allows safe flights in drape mode. Unmanned Aerial Vehicles (UAV) and Remotely Operated Vehicles (ROV) are even safer. The miniaturization technology for magnetic sensors and electronic systems (data acquisition, compensation, data transmission, etc.), automated flight control system and GPS navigation have enabled the design and development of drones of short range and long range cruising (Miles et al. 2008). The first UAV survey was operated in 2004 with high endurance, more than 10 hours at a speed of 75 km h^{-1} (Anderson and Pita 2005). Recent UAV, with 3-m wingspan and 18 kg mass, are more powerful with an endurance of 15 h and can travel at 100 km per hour. These UAV can be operated from sites near survey areas or from marine vessels. The main limitation for most of the UAV is their control by Line of Sight Communications. A remote operator near the region being flown is thus still required. New capabilities include autonomous tridimensional flight paths, long-range continuous satellite telemetry of geophysical data and flight parameters, radar altimeter and cooperative aeromagnetic surveying using teams of UAV controlled from a single ground station (Exploration trends & Development, 2005; Lum et al. 2005).

4.4 Data Acquisition and Reduction

4.4.1 Instrumentation

The geomagnetic field being a vector, magnetometers can be divided into two categories that differ both in terms of functionality and principle of operation. Vector magnetometers measure the magnetic induction value in a specific direction in 3-dimensional space whereas scalar magnetometers measure only the magnitude of the field regardless of its direction. Vector magnetometers are often mainly used as variometers, particularly in geomagnetic observatories, whereas scalar magnetometers are generally used as absolute instruments. In survey applications, one of the earliest instruments used was the Swedish mining compass developed in the mid-nineteenth century (Nabighian et al. 2005). This device resulting from the modification of the mariner's compass is based on a light suspended needle. It measures the inclination I and the declination D of the field. The revolution in geomagnetic surveys, at least for airborne magnetometers, came with the advent and development of the earth inductor (Logachev 1947; Heiland 1953; Reford and Sumner 1964). Various components of the magnetic field could then be measured from the electric voltage induced in the rotating coil. Nowadays magnetometers are not based on magnetic needles but use quantum mechanics properties of the atoms and nuclei for scalar magnetometers (Telford et al. 1990) and on ring-core saturation of a high magnetic permeability alloy for vector magnetometers (Muffly 1946; Vacquier 1946; Wyckoff 1948). The picoTesla precision and sensitivity reached nowadays are unprecedented.

4.4.2 Fluxgate Magnetometers

The airborne fluxgate magnetometer was originally designed and developed in 1941 by Victor Vacquier (Wyckoff 1948). It was built for use from low-flying

aircraft as a detection device for submarines during World War II. After modification of the airborne instrument, it was also a first ship-towed instrument for marine magnetic surveys. It became apparent that the device had possibilities for studying geologic features. Many airborne magnetic surveys were carried out using fluxgate detectors between 1945 and 1985.

A fluxgate magnetometer consists of two identical soft magnetic cores. Special low noise core material, usually μ-metal or Permalloy (Vacquier 1946), with high magnetic permeability and low energy requirements for saturation, are used to obtain very sensitive fluxgates with a low level of noise. These cores are wound with primary and secondary coils and are mounted in a parallel configuration with the windings in opposition. An alternating current (AC) of frequency f (50 to 1000 Hz) is passed through the primary coils, generating a large, artificial, and varying magnetic field in each coil. This field drives periodically the cores into saturation. This coil configuration produces induced magnetic fields in the two cores that have the same strengths but opposite orientations at any given time during the current cycle. If the cores are in an external magnetic field, such as the Earth's Magnetic field, the component of the external field parallel to the artificial field reinforces it in one of the cores. It is anti-parallel in the other core, reducing the artificial field. As the current and the artificial field strength increase, saturation will therefore be reached at different times in the two cores. When the electric current decreases, the two cores fall below saturation at different times. These differences are sufficient to induce a measurable voltage in a secondary detection coil at a frequency $2f$. The detected signal is proportional to the strength of the magnetic field in the direction of the cores. This type of magnetometer has an accuracy of about 0.5 nT to 1 nT but has a wide dynamic range. A modern version of this type of magnetometer includes three-axis fluxgate magnetometers designed for vector measurements. They are also suitable for magnetic compensation in planes. It should be mentioned that fluxgate devices have been intensively used in near Earth orbiting geomagnetic satellites since Magsat (Acuña et al. 1978; Langel et al. 1982), Oersted (Nielsen et al. 1995, 1997) and CHAMP (Reigber et al. 2002, 1999) but they are supplanted by scalar magnetometers for airborne applications (Paterson and Reeves 1985).

4.4.3 Nuclear Precession Magnetometers

Nuclear precession magnetometers polarize the atomic nuclei of a substance contained in a bottle by applying an electric current in the coil circling it. These nuclei starts precessing when the current is switched off. As the behavior of the nuclei returns to normal, the frequency of precession called the Larmor frequency of the nuclei is measured. It can be correlated to magnetic induction strength. Let us briefly review some of the common scalar nuclear precession magnetometers:

- Proton Precession magnetometers
- Overhauser Effect magnetometers
- Optical Pumping Alkali Vapor Magnetometers

4.4.3.1 Proton Precession Magnetometers

A proton precession magnetometer was developed by Varian Associates in the mid-1950s (Reford 1980) and very rapidly became the most popular magnetometer for all type of surveys (Reford 1980). It uses hydrogen as precessing atoms. Liquids such as water, kerosene and methanol can also be used because they all offer very high proton densities (hydrogen nuclei). A standard proton precession magnetometer uses a high intensity artificial DC around the sensor to generate a strong static magnetic field to polarize the protons. The polarizing DC current is then switched off which causes the protons in the liquid to precess around the ambient Earth's field as a top rotates and precesses around the Earth's gravity field. The Larmor frequency of the precession is proportional to the ambient magnetic field strength and the proportionality factor is called the nuclear gyro-magnetic ratio. This ratio depends only on fundamental constants and therefore proton precession magnetometers are absolute instruments. A simple coil can detect the precession signal of the protons. The signal lasts for 1–2 s. The power required to polarize the protons may be significant (Telford et al. 1990). Nevertheless, the standard proton precession magnetometer is by far the cheapest portable magnetometer. Its main advantages are its operating simplicity without the need for orientation of the sensor and a high accuracy (0.1 to 1 nT). For airborne applications its main limitations are related to its low sampling rate and limited dynamic range (Ripka 1996).

4.4.3.2 Overhauser Effect Magnetometers

Overhauser effect magnetometers (Overhauser 1953; Dobrin and Savit 1988) are based on the principle of nuclear magnetic resonance. They have been developed from the proton precession principle. An Overhauser magnetometer uses radio-frequency power to excite the electrons of a special chemical dissolved in the hydrogen-rich liquid. The electrons pass on their excited state to the hydrogen nuclei, altering their spin state populations, and polarizing the liquid, just like in a standard proton magnetometer but to a greater extent and with a much lower power requirement (Nabighian et al. 2005). Actually, the total magnetization vector of the hydrogen liquid is larger in an Overhauser magnetometer than in a proton precession magnetometer. This allows sensitivity to be improved. Since the liquid can be polarized while the signal is being measured, Overhauser magnetometers have a much higher speed of cycling than standard proton precession magnetometers. Overhauser magnetometers are efficient magnetometers available with high precision ($\sim$1 pT) and high sampling rate (10 samples per second) suitable for Earth's field measurements. However it should be noted that Overhauser as well as free proton precession sensors have signal to noise ratios (S/N) that are dependent upon the field strength conditions (Geometrics, Technical Report TR-120, 2000). In areas where the geomagnetic field is weak, in the south Atlantic for instance, their S/N deteriorates. The Overhauser magnetometer is commonly used onboard near-Earth geomagnetic satellite like Oersted (Nielsen et al. 1995) and CHAMP (Reigber et al. 2002).

4.4.3.3 Optical Pumping Alkali Vapor Magnetometers

The principle of optical pumping of electrons of a gas or a vapor was first described by Kastler (1954), then by Hawkins (1955) and by Dehmelt (1957). The concept of optical pumping is based on energy transition (or pumping) by circularly polarized optical-frequency radiation of electrons from one of two closely spaced energy levels to a third higher level, from which they fall back to both of the initial ground levels. The use of Zeeman transitions in the alkali metals for magnetometry was first suggested by Bell and Bell and Bloom (1957) using Sodium (and Potassium) vapor to detect the resonance. They suggested also the use of Rubidium or Cesium vapor. Potassium is also used in some magnetometers (Pulz et al. 1999). Recently Leger et al. (2009) described an absolute magnetometer based on ^{4}Helium to be used aboard the three satellites of the future near-Earth geomagnetic SWARM mission. We know from quantum physics that the electron can only take on a limited number of orientations with respect to the ambient magnetic field vector. Each of these orientations will have a slightly different energy level. This electron energy differentiation in the presence of an external magnetic field is called Zeeman splitting. The differences in energy from one Zeeman level to the next are proportional to the strength of the ambient field. It is these energy differences between the Zeeman levels that are measured to determine the Earth's magnetic field strength. For an ambient field of $\sim 50,000$ nT, the splitting energy will correspond to a frequency in the range of a few hundred kHz (Nabighian et al. 2005; Smith 1997; Parsons and Wiatr 1962). The frequency of resonance used was 700 kHz for the first alkali vapor magnetometers (Parsons and Wiatr 1962). Nowadays, the frequency of the oscillating signal varies between 70 kHz and 350 kHz whereas the free proton precession and Overhauser magnetometers use an oscillating signal of 0.9 kHz and 4.5 kHz respectively (Parsons and Wiatr 1962) (Geometrics, Technical Report TR-120, 2000). It is then clear that the higher frequencies of the optical pumping magnetometers as compared to precession magnetometers provide better response and reproduction of the magnetic field signal. Alkali vapor instruments have excellent sensitivity, better than 0.01 nT$(\sqrt{\text{Hz}})^{-1}$, and high sampling rate – values as high as 10 Hz – are commonly used in magnetic surveys (Nabighian et al. 2005). The comprehensive theoretical and technical descriptions of the alkali vapor optical pumping magnetometer may be found in Parsons and Wiatr (1962). A good discussion may also be found in Telford et al. (1990).

4.5 Survey Design

Aeromagnetic surveys are undertaken at the early stage of petroleum exploration before any other geophysical method (Reford and Sumner 1964; Reford 1980; Paterson and Reeves 1985; Nabighian et al.

2005). The aim was to determine the depth of the basement crystalline rocks underlying sedimentary basins. Sedimentary formations are assumed non-magnetic as their magnetic signal is very weak, below the resolution and accuracy of the measurements. The estimation of the basin thickness is thus indirectly derived. However, the steady improvement of magnetometer sensitivity, the high resolution and accuracy achieved by the magnetometers, and the very high accuracy (sub-metric) of the positioning systems allowed by dGPS (Parkinson and Enge 1996) make it possible nowadays to outline weakly magnetized layers. According to Paterson and Reeves (1985), very small variations in magnetite concentration inducing anomalies as low as 0.1 nT can be correlated with diagenetic processes in hydrocarbon accumulations, and some hydrocarbon-related structures can now be detected in weakly magnetic sedimentary rocks (Grauch and Millegan 1998). The discovery of many structural oil traps by this method within the Sichuan Basin in China is the most typical example (Zhana 1994). However regional and detailed aeromagnetic surveys continue to be primary mineral exploration tools. These surveys allow variations in the concentration of various magnetic minerals, primarily magnetite, to be mapped. Aeromagnetic methods are therefore indirect exploration methods as magnetite is only a "marking" element. The goal in aeromagnetic surveys is the search for mineralization such as iron-oxide-copper-gold deposits as well as skarns and massive sulfides or heavy mineral sands (Nabighian et al. 2005). One of the main applications is the recognition and delineation of structural or stratigraphic environments favorable for mineral deposits of various types such as carbonatites, kimberlites (as host rock for diamonds), porphyritic intrusions, faulting and hydrothermal alterations (Keating 1995; Allek and Hamoudi 2008; McCafferty and Gosen 2009). High resolution aeromagnetic surveys are therefore very powerful tools for general geologic mapping (Reynolds et al. 1990, Bournas 2001). Depending upon the geological problem to be addressed, its framework, and all the related economical, scientific and technical constraints, aeromagnetic surveys are flown with a wide variety of geometric and metrological characteristics. The geometrical characteristics are mainly the flight lines and control lines (Tie lines) spacing, and the terrain clearance, or barometric height, or height above mean sea level. The metrological characteristics are related to accuracy and resolution of the magnetometers, the sampling rates, and the positioning system. All these points, together with the recording of the magnetic field temporal variations at a base station, are fundamental in order to achieve high quality final mapping. More details are given in "Data acquisition Section 4.6".

4.5.1 Flight Direction and Line Spacing

During aeromagnetic survey design, the flight path direction is selected mostly on the basis of the geological strike. For general reconnaissance mapping purposes the flight lines are usually oriented along cardinal directions, north-south or east-west (Cordell et al. 1990; Horsfall 1997). In the case of more specific surveys related to mineral exploration, it is then preferred to orient the flight lines in the direction perpendicular to the geological strike to maximize the magnetic signature. Control lines (Tie lines) are flown perpendicular to flight lines to provide a method of eliminating temporal variation of the magnetic field using pairs of values recorded at the intersections. This process is called leveling. It will be further described in Section 4.8.3. As a rule of thumb the tie lines spacing is in general 10 times the profile lines spacing. In polar regions a rate of 5 to 1 is often adopted (Bozzo et al. 1994). Cordell et al. (1990) recommended this rate for United States of America Midcontinent aeromagnetic surveys. However, for some petroleum exploration the ratio may be as low as 3 to 1 (Horsfall 1997) or even 2 to 1 (Reeves 2005). In the past, line spacing of 3000 m was generally adopted for surveys over sedimentary basins. These kinds of surveys are now flown with 500 m line spacing (Cady 1990). Flight-line spacing was limited in the past to 1500 m over crystalline areas whereas they are now flown at 400–500 m or even 200 m. Surveys dedicated to mineral exploration are usually flown at 200 m line-spacing, sometimes as close as 50 m line-spacing for very high resolution exploration surveys (Horsfall 2). Flight-line spacing is generally determined by average depth to crystalline basement (Reid 1980; Cordell et al. 1990), by the degree of detail required in final mapping (Horsfall, 1997) and the size of the target to detect (Horsfall 1997; Reeves 2005). The financial resources available for the survey are also crucial in this choice. Reid (1980) showed that in order to avoid aliasing in the short wavelength of the signal, neither the flight-line spacing, nor inline sampling rate

should exceed twice the average target depth in total-intensity surveys. These results were obtained using spectral analysis and the power spectrum expectation relationship of Spector and Grant (1970). Equivalent analysis for the gradiometer surveys led Reid (1980) to recommend flight-line spacing equal to the average depth to crystalline basement. The sampling rate of the modern magnetometers is very high, up to 1 kHz. Generally, the speed of the aircrafts used is not a limitation to achieve the expected resolution of the mapping. Indeed, the aircraft speed used during the surveys varies between 220 and 280 kmh^{-1} – typically 250 kmh^{-1} – corresponding to about 69 ms^{-1}. Using a modern magnetometer with a sampling rate of 10 Hz, the along line spacing is then around 7 m (Horsfall 1997; Reeves 2005). The achieved sensitivity of the Alkali Vapor Optically Pumped Magnetometers is of the order of 0.01 $nT(\sqrt{Hz})^{-1}$. To benefit from such a high accuracy and achieve high resolution field mapping, it becomes crucial to be able to remove the signal due to other sources of noise, like aircraft magnetic interference (Hardwick 1984a, b).

4.5.2 Survey Flight Height

Let us recall that the magnetic field decreases as the inverse cube of the distance from the magnetic source to the sensor, at least for elementary dipolar sources. Therefore to detect small variations in the magnetic field, surveys must be flown close to the ground. The magnetic sources may be covered by non-magnetic material and the ground clearance is the distance between the sensor and the Earth's surface. Regional mineral/petroleum surveys were usually flown in the 1970s at a constant ground clearance of 150 m (Horsfall 1997; Bournas 2003; Allek and Hamoudi 2008). Table 4.1 shows the line spacing and corresponding height used for recent aeromagnetic surveys

The main limitation on the survey height is related to flight safety. Aircraft performance is the main factor in maintaining ground clearance. In areas with highly varying topography, or rugged terrain, fixed-wing aircraft may not be suitable for surveys. Whenever possible financially, helicopter are by far the best platform to use in rugged terrain to keep a small ground clearance. Regional geological purpose surveys might be conducted at higher altitudes ranging from 500 to 1000 m with appropriate line spacing, but then, only broad features will be outlined (Reid 1980).

Table 4.1 Survey lines spacing and corresponding height values (From Horsfall 1997)

Line spacing (m)	400	200	100
Height (m)	100	80	60

4.6 Data Acquisition

Airborne magnetic survey quality has benefited from technological developments and miniaturizing devices. The amount and variety of data collected during an airborne survey is so large, due to the fast sampling rate achieved, that a computer is necessary for acquisition and storage. Analog magnetic data are digitized and stored (either in a data logger or in the computer). The navigation data necessary for flight-path and data recovery for geophysical field mapping are also stored. The flight paths are nowadays recorded on a color video camera (Fig. 4.1). The flight-path tracking cameras and aerial photographs used in pre-GPS and radio era were an essential component of coordinate and flight-path recovery (Le Mouël 1969; Luis 1996; Horsfall 1997). Indeed they were time synchronized to geophysical data via an onboard timer. The accuracy achieved with such tracking systems ranges between 50 m and 1 km for horizontal coordinates. With the help of radio navigation or inertial devices the vertical accuracy was improved to about 30 m (Le Mouël 1969). For low altitude mineral/petroleum exploration, radar altimeter led to accuracy of the order of ± 10 m in the mid-seventies (Allek and Hamoudi 2008), whereas ± 1 m accuracy can easily be reached with modern devices (Reeves 2005). The altimeter data are used to validate each crossover during tie-line leveling of the magnetic data.

With GPS navigation there is no need for video recording in flight-path recovery. It is mainly used for a posteriori checking of the accuracy of the navigation (Horsfall 1997) and in the case of special "cultural" signatures appearing in the geophysical data. GPS not only provides a very accurate positioning system especially in its differential technique (dGPS) (Parkinson and Enge 1996) but also very accurate time reference. This time is synchronized with geophysical data and recorded on the data acquisition system.

Fig. 4.1 The onboard aircraft data acquisition system mounted on a rack for airborne geophysics (Courtesy of Geometrics)

Moreover, the synchronization with the base station where the geomagnetic field is continuously recorded is essential for removal of the daily diurnal field variation from the total-field recorded onboard the aircraft. The data acquisition system, as presented in the Fig. 4.1, incorporates a monitor where outputs from the real-time geophysical and navigation instruments are displayed and a monitor associated with a color video camera. The present data acquisition equipment is almost self autonomous and need only be programmed before take-off so that surveys are often flown with only the pilot onboard. This policy allows longer survey flights (Reeves 2005). The actual accuracy and resolution really achieved in an airborne survey is dramatically reliant on the aircraft navigation system used. The constant ground clearance normally specified for the survey requires altitude measurement. Survey aircrafts are then fitted with radar altimeters beside the classical barometric altimeter. The data of these altimeters are also recorded by the data acquisition system. When combined with the aircraft GPS height, the radar altimeter allows the 3D flight path and the Digital Elevation Models (DEM) of the area being flown to be derived. For the very high-resolution surveys, a laser altimeter is also added onboard. Measurements undertaken in draped mode have considerably improved and they have become almost a standard in both heliborne and fixed-wing magnetic surveys. Pre-computed heights along the flight line in the new versions of navigation software let the pilot follow the draping more effectively and safely than the previous intensive computer's CPU time versions where the position along the profile was computed in real-time from grids (Exploration Trend & Development in 2008).

4.6.1 Magnetic Compensation of Aircraft

Two configurations are possible for the sensors of an airborne magnetic survey. In the first, and classical one, the magnetic sensor is located in a bird and towed as far as possible below the aircraft to reduce its magnetic effect. In the second configuration, the magnetic sensor is fixed to the aircraft either in a tail stinger (Fig. 4.2) or

Fig. 4.2 Magnetometer sensor in a stinger (*top*) on a tail of a Piper Navajo aircraft and (*bottom*) on a Bell helicopters (Courtesy of Novatem)

on the wingtip in the horizontal gradiometer configuration. A fixed installation of a total field magnetometer sensor on an aircraft is much more desirable than the towed bird configuration first for safety reasons and second because the bird configuration is not error or noise-free. The fixed configuration usually shows the best signal-to-noise ratio provided that all the magnetic disturbing effects of the aircraft are removed or compensated (Horsfall 1997; Reeves 2005).

Let us assume that the total field $B(P,t)$ measured at time t and point $P\,(x,y,z)$ by an airborne magnetometer in the fixed-sensor configuration may be modeled as the sum of three components (Williams 1993):

$$B\,(P,t) = B_i\,(x,y,z,t) + B_e\,(x,y,z,t) + B_{\text{dist}}\,(\theta_1,\theta_2,\theta_3) \tag{4.1}$$

where B_i is a function of space and time and represents the intensity of the Earth's magnetic field at a point P. The three angles $\theta_1,\theta_2,\theta_3$ are the plane heading, roll and pitch respectively.

This is the quantity of interest in the survey while both the remaining terms may be considered as disturbances or interferences. The function B_e varies with time and represents the diurnal variation (or transient external magnetic field). It varies significantly during the survey flight but is considered uniform in a limited area around the base station where the magnetic field is recorded simultaneously. The third function B_{dist} is the disturbance field generated by the aircraft. This disturbance field is a function of the attitude of the aircraft. Among all the disturbances the most significant are:

(1) Its remnant magnetization – i.e., permanent magnetic effects B_{perm}
(2) Its induced magnetization generated by the Earth's magnetic B_{ind}
(3) Eddy currents caused by the electrical conductor moving through the Earth's magnetic field and their magnetic effects B_{eddy}.
These effects are not easy to compensate and the solution is to move the sensors away from these sources.
(4) Magnetic effects of electric currents from the instruments, generators and avionics. Shielding and grounding the electric cables reduce these effects. The first three magnetic interference sources should be minimized in order to produce reliable magnetic data that can be related to geological features. This minimization is called "magnetic compensation of the aircraft". Two approaches have been proposed to mitigate these disturbances (Hardwick 1984a, Williams 1993). The first approach called "passive magnetic compensation" uses permanent magnets at various places (Geometrics, MA-TR15 technical Report). This method is however a trial-and-error method. It is time-consuming and moreover it does not compensate for motion of the aircraft (Reeves 2005). The second approach proposed by Leliak (1961) is referred to as "active" and uses a compensator. The system was originally designed for use with military magnetic detection systems. Leliak (1961) proposed building an analytical model of the disturbances (Williams 1993; Gopal et al. 2008; Pang and Lin 2009). Let us assume that the disturbance field may be written as:

$$B_{\text{dist}} = B_{\text{perm}} + B_{\text{ind}} + B_{\text{eddy}} \tag{4.2}$$

With

$$\begin{aligned}
B_{\text{perm}} &= a_1\cos X + a_2\cos Y + a_3\cos Z\\
B_{\text{ind}} &= a_4B_t + a_5B_t\cos X\cos Y + a_6B_t\cos X\cos Z\\
&\quad + a_7B_t\cos^2 Y + a_8B_t\cos Y\cos Z\\
&\quad + a_9B_t\cos^2 X\\
B_{\text{eddy}} &= a_{10}B_t\cos x\dot{\cos} X + a_{11}B_t\cos X\dot{\cos} Y\\
&\quad + a_{12}B_t\cos X\dot{\cos} Z + a_{13}B_t\cos Y\dot{\cos} X\\
&\quad + a_{14}B_t\cos Y\dot{\cos} Y + a_{15}B_t\cos Y\dot{\cos} Z\\
&\quad + a_{16}B_t\cos Z\dot{\cos} X + a_{17}B_t\cos Z\dot{\cos} Y\\
&\quad + a_{18}B_t\cos Z\dot{\cos} Z
\end{aligned} \tag{4.3}$$

where $\cos X$, $\cos Y$ and $\cos Z$ are the direction cosines of the Earth's magnetic field along the longitudinal, transverse and vertically down instantaneous major axes of the aircraft respectively while $\dot{\cos} X$, $\dot{\cos} Y$ and $\dot{\cos} Z$ represent their first time derivatives. These direction cosines are defined as:

$$\begin{aligned}
\cos X &= \tfrac{T}{B_t}\\
\cos Y &= \tfrac{L}{B_t}\\
\cos Z &= \tfrac{V}{B_t}
\end{aligned} \tag{4.4}$$

where T, L, and V are the components of the total field B_i along traverse, longitudinal and vertical axes of the aircraft respectively. T is positive to port, L is positive forward and V is positive downward (see Fig. 4.3). The

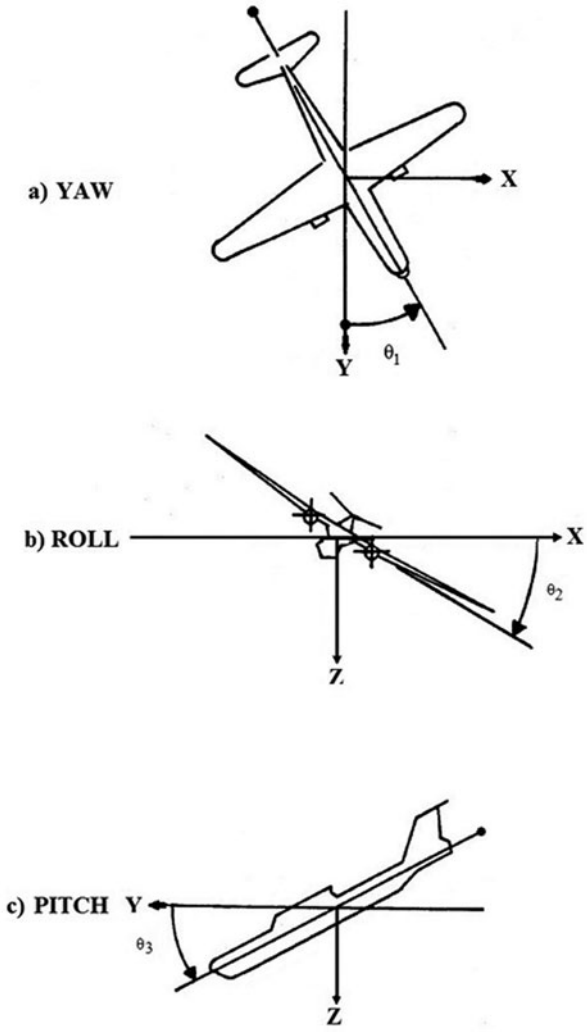

Fig. 4.3 The attitude Yaw, Roll and Pitch angles of the moving platform, in the transverse, longitudinal and vertical axes. Modified from Rice (1993)

determination of the 18 coefficients of Eq. (4.3) gives the magnetic field compensation. Hardwick (1984a) suggests adding a DC term for full compensation. Different numerical methods (ridge regression, least-squares, neural network, FIR model...) have been developed. Commercial compensators (Fig. 4.1) are based on such algorithms. Vector measurements are however necessary to solve the problem. A fluxgate vector magnetometer is added to the payload and must be rigidly mounted in a magnetically quiet location of the aircraft, far from the engines. In some configurations, the fluxgate is mounted in the middle section of the tail stinger. An active compensator is then composed of:

- Three-component fluxgate vector magnetometer.
- Multi-channel data acquisition and signal processor circuitry, to record signals from the scalar (Cesium, protons or Helium type) and vector magnetometers, GPS differential receiver board, Analog processor board.
- A main microcomputer with software, real-time clock, digital output.

Magnetic compensation for aircraft and heading effects is done usually in real-time. Raw magnetic values are also stored for later use if necessary. Active magnetic compensation begins with a calibration phase where all the magnetic interference values are determined in the absence of local magnetic anomalies. This undertaken at high altitude, generally between 1000 and 4000 m (Williams 1993; Reeves 2005) to minimize the influence of any local magnetic anomalies on the data following a specific geometry. To define the response of the aircraft in the Earth's magnetic field during the maneuvers, one has to derive a set of coefficients using magnetic data from scalar magnetometer and the attitude data from the fluxgate. Typical compensation maneuvers consist of a series of pitches, rolls, and yaws on four orthogonal headings (Hardwick 1984a; Reeves 2005) with 30 to 35 degree bank turns between each heading. This calibration procedure takes about 6 minutes of flying time (Hardwick 1984a; Reeves 2005). The standard amplitudes for aircraft attitude parameters are Pitch of $\pm 5°$, roll of $\pm 10°$ and yaw of $\pm 5°$. Each individual maneuver lasts about $30s$. The angles are relatively small which allow to use approximation of their trigonometric functions, i.e. $\sin\theta_i \approx \theta_i$ and $\cos\theta_i \approx 1 - \theta_i^2/2$. The compensation maneuvers are flown each time a new compensation is required, for instance if the magnetic field characteristics over a survey area are new. The effectiveness of the compensation is usually evaluated by the "Figure of Merit" (FOM) (Hardwick 1984a; Reeves 2005). The FOM is defined as the absolute sum of the total intensity anomaly measurements, along the four cardinal directions and compensated for the plane signal. In the seventies, a FOM of 12 nT was typical for regional surveys (Reeves 2005) whereas it has decreased nowadays from below 1 nT down to 0.3 nT after compensation (Horsfall 1997; Ferris et al. 2002).

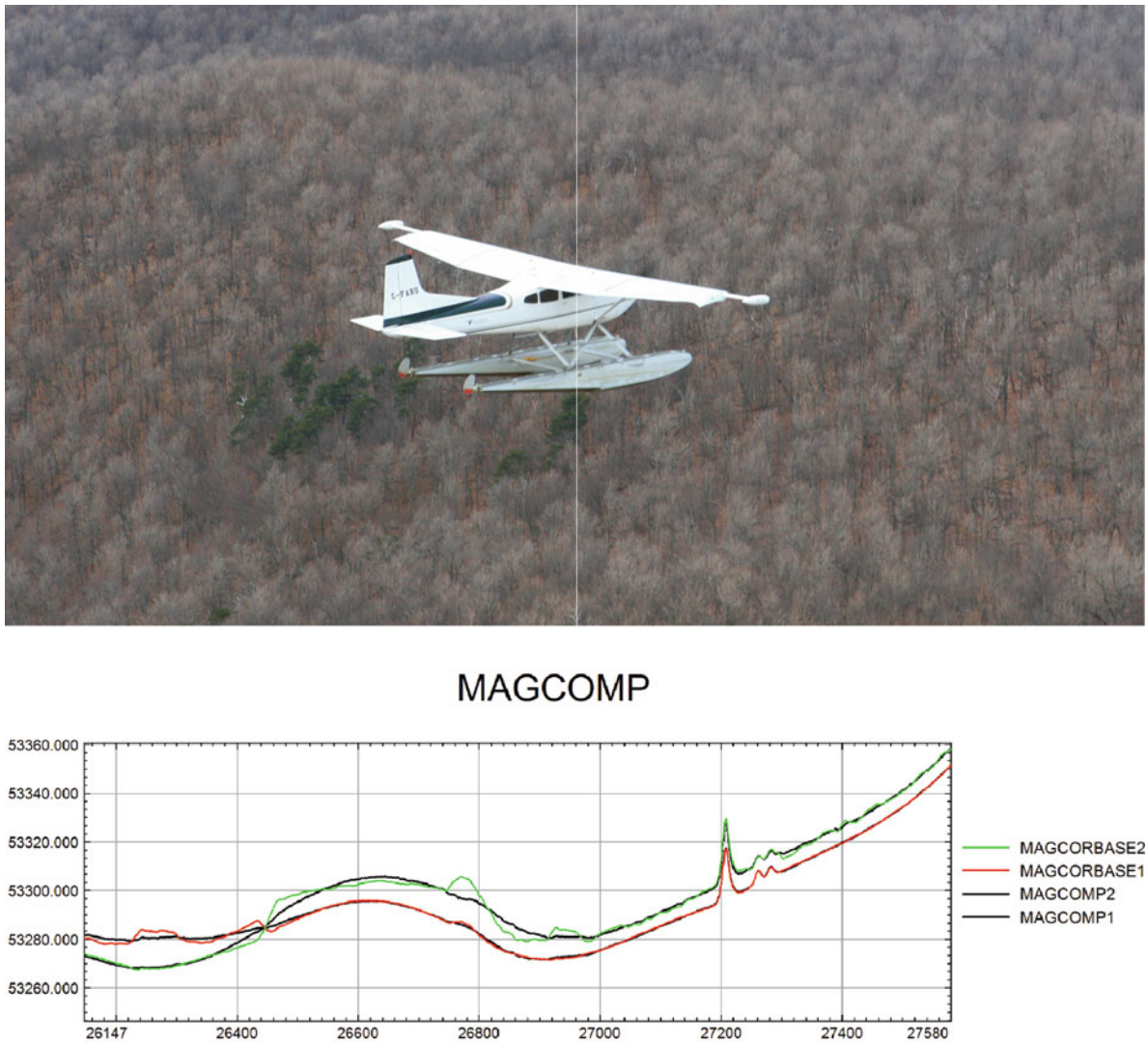

Fig. 4.4 Compensation effect of the interference generated by the aircraft on the two sensors located on wing-tip pods of aircraft (*top*). Red and green curves are uncompensated raw data and black curves are compensated data (*bottom*)(Courtesy of Novatem)

The magnetic component generated by the heading error of the aircraft is reduced to less than 1 nT. The calibration response is then stored in the memory of the compensator and subtracted from the incoming data during the survey operation (Horsfall 1997; Reeves 2005). Figure 4.4 illustrates the compensation effect on the data recorded by the two high-resolution magnetic sensors located in the wing-tip pods for measurements of the horizontal gradient.

4.7 Data Checking and Reduction

Digital recording and processing are nowadays commonly used in airborne surveys. The traditional relationship between those who are collecting and compiling data, and those who are using and interpreting these data has slightly changed. It is very easy to digitally handle the huge amount of collected data during

the survey but great care has to be taken when checking data to avoid introducing false anomalies (Reford 1980). There is usually a two-step data verification, the first is the in-flight checking and the second after the flight.

4.7.1 In-Flight Data Checking

The data from the magnetometer(s), altimeter(s) and navigational system are displayed either on the monitor or on the graphic printer outputs when available onboard the aircraft and should reveal any major in-flight problem (Horsfall 1997).

4.7.2 Post-Flight Checking

At the end of each day, the data recorded onboard are verified and preliminary analyses are undertaken.

(a) Statistical analysis of each line flown and potential problem detection are among the first analyses performed.
(b) Detection and isolation of spikes and spurious recording (Fig. 4.5) are important for the data quality. This detection is usually based on the fourth-difference operator according to the following equation:

$$\Delta Q_i = Q_{i-2} - 4Q_{i-1} + 6Q_i - 4Q_{i+1} + Q_{i+2} \tag{4.5}$$

where Q is any measured quantity onboard the aircraft (uncompensated or compensated magnetic field data, Radar altimeter data or Barometric altimeter data) or at the base-station. The datum is considered valid if the operator returns a result less than a fixed threshold. The appropriate choice of threshold value is empirically determined.
(c) Calibration test line to ensure that equipment is operating within tolerances.
(d) Detection of any high frequency magnetic anomalies generated by any "cultural" anthropogenic noise like pipelines or railways (Horsfall 1997; Reeves 2005) is done. The video recording during flight-line data acquisition may be of great help to identify the perturbation sources.
(e) Checking the compliance of the flight path with survey specifications is necessary.
(f) The base station is checked to ensure the diurnal variation stays within the survey specifications.

It should be emphasized that partial or total re-flying will occur if one or more of the following conditions holds:

- The magnetic diurnal variation exceeds the survey specifications
- The aircraft's speed derived from the GPS navigation system is abnormal

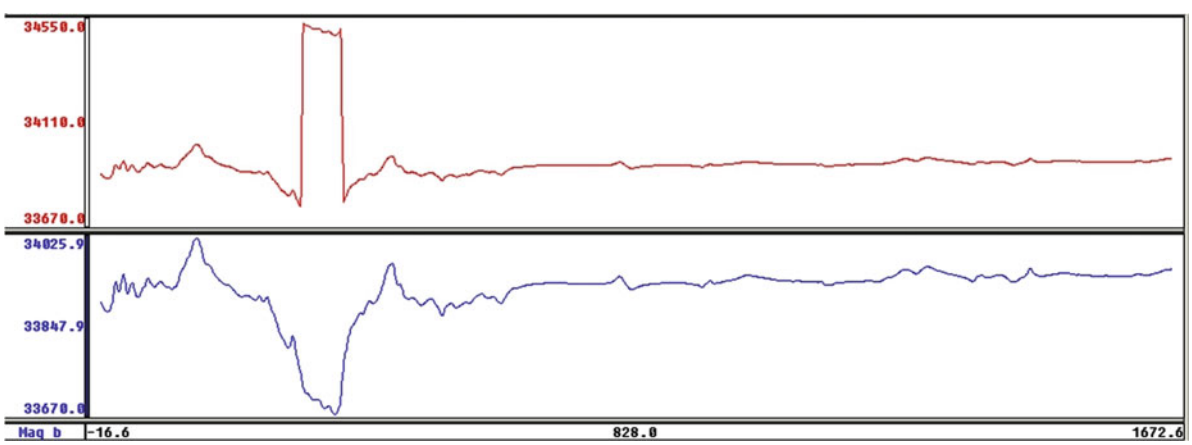

Fig. 4.5 Detection of spurious data along a line (*top*) in post-flight checking and correction (*bottom*). Units are nT for total field and kilometers for distance along flight line

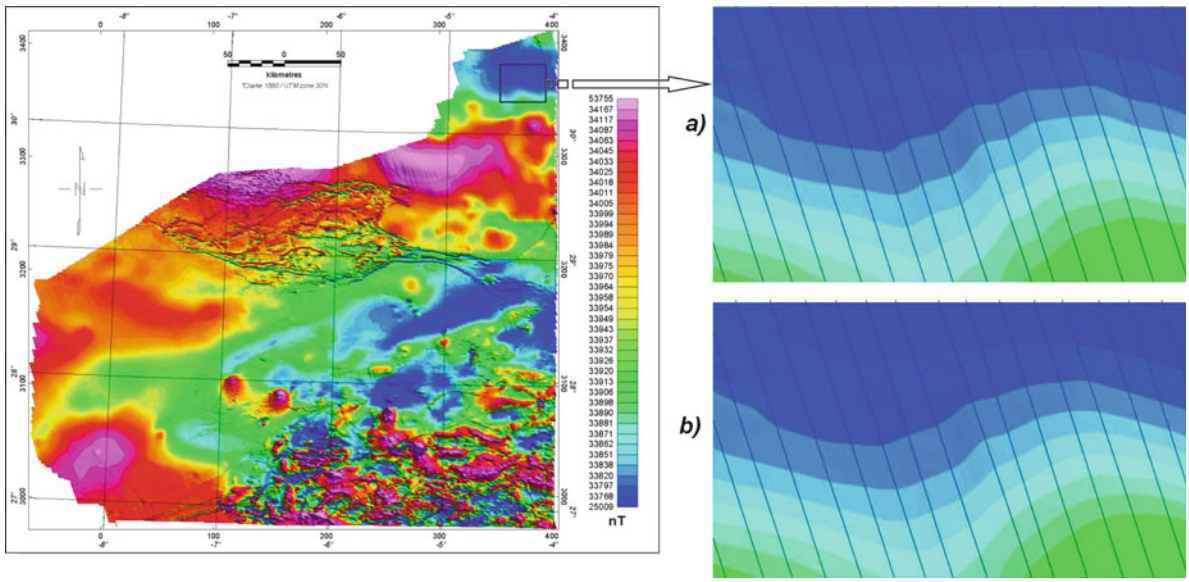

Fig. 4.6 lag effect correction of the magnetic field in the towed bird sensor configuration. (**a**) Raw data. (**b**) Corrected data (after Allek (2005))

- Final differentially corrected flight path deviates front the intended flight more than the survey specifications.
- The final differentially corrected altitude deviates from the flight altitude specifications.

In addition:

- Magnetic data channels contain multiple spikes.
- GPS data shall include at least four satellites for accurate navigation and flight path recovery.
- There should be no significant gaps in any of the digital data, including GPS and magnetic data.

After checking the continuity and integrity of the data, correcting the on-board recorded data (flight path, time, and geophysical data) and importing base station data, a database is created. The data are posted to the database on a flight by flight basis. The final steps in the daily processing of the data after validation are:

- Producing diurnally corrected airborne reading. For this, the base level value of the base station magnetic data has to be estimated. It is then subtracted from the digital diurnal data and the resultant values are added to the time synchronized digital onboard magnetic data.
- Merging of the geophysical data and navigational (aeronautical) data (geographic location, time)

The procedures described above are daily duties throughout of the survey. Data should be validated by the technical certifying authority in charge of the project (Reeves 2005) before ending the survey. The global database containing all the relevant information related to the survey is then created. In the case of towed bird magnetic sensor configuration, magnetic data should be corrected for the lag effect that is responsible for the "zigzag" shape perturbation of the anomaly field (Fig. 4.6). Further processing is however needed before gridding and mapping the magnetic anomaly field.

4.8 Data Processing

4.8.1 Magnetic Anomaly Field Determination

Let us recall that the "vector magnetic anomaly field" is the magnetic induction generated by the rock

magnetization (or susceptibility) heterogeneities of the Earth or planetary crust. In the case of the Moon, this quantity has been directly measured on some sites by the Apollo Astronauts. This is because the Moon, unlike the Earth, does not have a global internal field (Ness 1971). In the case of the Earth, the geomagnetic field is clearly dominated by the core's contribution, which represents almost 99% of the amplitude of the internal signal. The total intensity of the internal magnetic field (i.e., magnitude of the combination of the core and crustal fields) has then to be measured very accurately in order to be able to recover the crustal field. Let us consider an orthonormal cartesian coordinate system (O, x, y, z) where O is the origin of the system, and the axes Ox, Oy and Oz are respectively directed toward the geographic North, the East and Downward. The crustal sources lie in the lower half-space ($z > 0$). We assume also that the survey area – call it the domain D – belonging to the upper half space is of limited extent so that the planar approximation holds. If the survey area is too large for this approximation to be valid, the survey area can be divided into small pieces to fulfill this requirement. At any point $P(x, y, z)$ of D, the instantaneous total magnetic field measured at time t may be expressed as:

$$\mathbf{B_t}(P,t) = \mathbf{B_N}(P,t) + \mathbf{B_a}(P,t) + \mathbf{B_e}(P,t) \qquad (4.6)$$

where: $\mathbf{B_N}$ is the core field or normal field, also called the main field, $\mathbf{B_a}$ is the crustal field or anomaly field and $\mathbf{B_e}$ is the transient external field. It is worth recalling that the amplitude of the main field varies from roughly 20000 nT to 65000 nT from the equator to the pole respectively. Its modeled spatial wavelengths vary from 2500 km to 40000 km. Its time variation, called secular variation, has to be taken into account in two cases: (1) if panels of adjacent surveys based on data collected and processed at different epochs have to be merged. (2) if the survey time span exceeds a year. The external field varies from some few 10^{-3} nT to some 10^{3} nT during magnetic storms and from 10^{-3} s characteristic time scale to 22 years for the solar cycle (Cohen and Lintz 1974; Courtillot et al. 1977). During magnetically disturbed days, acquisition should stopped. Typically, a day is disturbed if the diurnal activity is greater than 5 nT over a chord of 5 min in length. Sometimes values of 2 nT over 30 s are used. The most important external magnetic field contribution that is necessarily recorded during ground or airborne surveys is the diurnal variation.

4.8.2 Temporal Reductions/Corrections

When there is no permanent geomagnetic observatory available in their vicinity, airborne and land surveys generally include a base station magnetometer that continuously samples the magnetic field time variations during the data acquisition flight period. Usually, the fixed station is operated in the centre of the surveyed area. It is still a matter of debate on how many base stations are needed for large surveys in order to adequately represent the highly varying diurnal magnetic field. The problem was first pointed out by Whitham and Loomer (1957) and Whitham and Niblett (1961) (see Nabighian et al. (2005)). This problem is even more difficult to handle in the case of marine measurements or airborne surveys over oceanic areas (Luis 1996; Luis and Miranda 2008). When it is not necessary to recover the total field, it is then simpler to use a gradiometer technique rather than a single sensor magnetometer. In this multi-sensor configuration (Fig. 4.4), the common features – i.e., normal field and external time varying field – are removed by calculating the differences between the signals recorded at different instruments. With the significant improvements in aeromagnetic survey instrumentation (resolution of magnetometers less than 0.1 nT and high precision positioning systems with an accuracy of less than a meter) and processing, the assumption of uniform temporal magnetic variations is only partially justified (Reeves 1993). Clearly, in some specific areas like those under the influence of the Equatorial Electrojet (EEJ), the non-uniformity of the temporal variations should be taken into account for data correction (Rigoti et al. 2000). The uncorrected effect of the EEJ, after subtraction of the base station data was reported by Rigoti et al. (2000) to amounts to 70 nT over a distance of 250 km (or 0.28 nT km^{-1}). This gradient may be as large as 1 nT km^{-1} (Rigoti et al. 2000). Close to auroral zones, or areas with high electric conductivity, where induction effects may be important (see for example Milligan et al. (1993)), the temporal variations may be considered uniform only for very short distances, not exceeding 50 km from the base station.

Let us assume that transient external magnetic field variations are zero-mean when averaged over a long time interval, at least a year. Then, the values of corrected for time variations may be derived using the data collected at the base station and at the nearest magnetic observatory. This procedure has been described by Le Mouël (1969) and used for example for the Azores Island aeromagnetic survey by Luis et al. (1994). Let us briefly recall the relationship to be used for correcting the data for these effects. First, let us denote O for observatory, S for Base-station and P for any given point in space where the total-field is measured. We note $\bar{B}_t^{\,\mathrm{an}}(O)$ and $\bar{B}_t^{\,\mathrm{sur}}(O)$ the annual mean and survey time-interval mean of the total-field at a given observatory O close to the domain D. The $\bar{B}_t^{\,\mathrm{an}}(S)$ and $\bar{B}_t^{\,\mathrm{sur}}(S)$ are the corresponding means at the base-station S. $\bar{B}_t^{\,\mathrm{an}}(P)$ is the annual mean at any measurement point P along the flight lines. Following Le Mouël (1969) two simplifying assumptions are necessary for time variation corrections. The first one assumes that the transient variations are the same at the base-station and at the measurement point P of D, which gives:

$$B_t(P,t) - \bar{B}_t^{\,\mathrm{an}}(P) = B_t(S,t) - \bar{B}_t^{\,\mathrm{an}}(S) \tag{4.7}$$

The problem is then to compute $\bar{B}_t^{\,an}(S)$ when the duration of the survey is less than a year. This done by assuming that:

$$\bar{B}_t^{\,\mathrm{sur}}(S) - \bar{B}_t^{\,\mathrm{an}}(S) = \bar{B}_t^{\,\mathrm{sur}}(O) - \bar{B}_t^{\,\mathrm{an}}(O) \tag{4.8}$$

i.e., by assuming that the differences of the mean between the base-station S and the closest observatory O, due to the time difference, are the same. The combination of (4.7) and (4.8) leads to:

$$\bar{B}_t^{\,\mathrm{an}}(P) = (B_t(P,t) - B_t(S,t)) + (\bar{B}_t^{\,\mathrm{sur}}(S) - \bar{B}_t^{\,\mathrm{sur}}(O)) + \bar{B}_t^{\,\mathrm{an}}(O) \tag{4.9}$$

Equation (4.9) is convenient to derive to a common epoch the static total field at any points P of the domain D. In order to use the Eq. (4.9), it is necessary to have either an observatory or a repeat station nearby (Le Mouël 1969; Chiappini et al. 2000; Supper et al. 2004) to estimate the mean field and the secular variation values. In the case where no observatories or repeat stations are available, different approaches have been proposed. As an example, in the case of the aeromagnetic survey of the Azores Islands, Luis (1996) suggests approximating the mean observatory values $\bar{B}_t^{\,\mathrm{an}}(O)$ and $\bar{B}_t^{\,\mathrm{sur}}(O)$ by their corresponding values derived from the International Geomagnetic Reference Field (IGRF) models (for details about the IGRF and other reference field, refer to section 4.9). Then the general equation reduces to:

$$\bar{B}_t^{\,\mathrm{an}}(P) = (B_t(P,t) - B_t(S,t)) + (\bar{B}_t^{\,\mathrm{an}}(S) - \bar{B}_t^{\,\mathrm{sur}}(S))_{IGRF} + \bar{B}_t^{\,\mathrm{sur}}(S) \tag{4.10}$$

The quantity defined in (4.11) below, is a good approximation of the "secular variation" of the main magnetic field over the area of interest.

$$\delta B(S) = (\bar{B}_t^{\,\mathrm{an}}(S) - \bar{B}_t^{\,\mathrm{sur}}(S))_{IGRF}/\Delta t \tag{4.11}$$

where Δt is time interval of the survey. The temporal corrections to apply to sampled data in order to derive the total field are given by:

$$\bar{B}_t^{\,\mathrm{an}}(P) = (B_t(P,t) - B_t(S,t)) + \bar{B}_t^{\,\mathrm{sur}}(S) + \delta B(S).\Delta t \tag{4.12}$$

The Eq. (4.9) described above is valid in a general framework. It can be used for surveys of limited geographic extension and/or flown over short time span. However it is used in a simplified form for helicopter-borne surveys and for surveys performed within a radius of approximately 50 km (Paterson and Reeves 1985) and up to 100 km (Whitham and Niblett 1961; Le Mouël 1969) of the base-station. Such surveys are typically those for oil and mineral exploration. Indeed, in these cases the time-corrected field is simply defined by:

$$B_t(P) = (B_t(P,t) - B_t(S,t)) \tag{4.13}$$

where measurements along the flight-lines and at the base-station are time-synchronized. Assuming that the total-field magnetic anomaly distribution is time-invariant, the values obtained at the intersections between flight-lines and control-lines should be almost the same. Any significant difference is then attributed to uncorrected temporal variation.

4.8.3 Magnetic Leveling

As previously described, aeromagnetic surveys are flown according to a designed and planned network (Reeves 1993) of flight-lines (L) and almost orthogonal control-lines also called Tie-lines (T). The Tie-line spacing is generally greater than the one for flight-lines. As a rule of thumb a rate of 10 to 1 is usually used while 5 to 1 is adopted in high latitude regions (Bozzo et al. 1994). In areas where geologic features lack a dominant strike, a rate of 1 to 1 has been used (Nabighian et al. 2005). This network provides a mean to assess the quality of temporal data reduction. The differences at the intersecting points of the network should be close to zero if the coordinates of the points are accurately determined in each direction (Paterson and Reeves 1985; Reeves 1993; Nabighian et al. 2005) as is generally the case for modern positioning systems like dGPS. Because the L-T differences at the intersection points are usually not negligible (Fig. 4.7), different empirical strategies have been developed to minimize the closure errors.

The process introduced to minimize these errors is called magnetic leveling. It was originally developed as an alternative to the use of base station data reduction (Whitham and Niblett 1961; Reford and Sumner 1964; Foster et al. 1970; Mittal 1984). The most common procedure is probably the two step method. The first step is a linear first order correction. A constant correction is calculated, based on the statistical mean of the closure errors or determined by least-squares minimization and distributed equally to each data point along the lines. In the second step a low order polynomial correction is adjusted to reduce the mis-ties below a specified minimum, usually 0.01 nT (Reeves 1993; Bozzo et al. 1994, Nabighian et al. 2005). Some algorithms consider tie-lines as fixed and adjust only the flight-lines. In the pre-GPS era, the L-T leveling errors were characterized by high amplitude values up to 20 nT with zero average. The achieved differences are now commonly of a few nT with an average over the length of a line of the order of 3 nT for a small extent or helicopter-borne survey (Reeves 1993). Once the leveling is complete, the total field may be gridded (Bhattacharyya 1971; Briggs 1974; Hansen 1993) and contoured using any available technique of digital enhancement provided that the data distribution is dense over the surveyed area (Fig. 4.8).

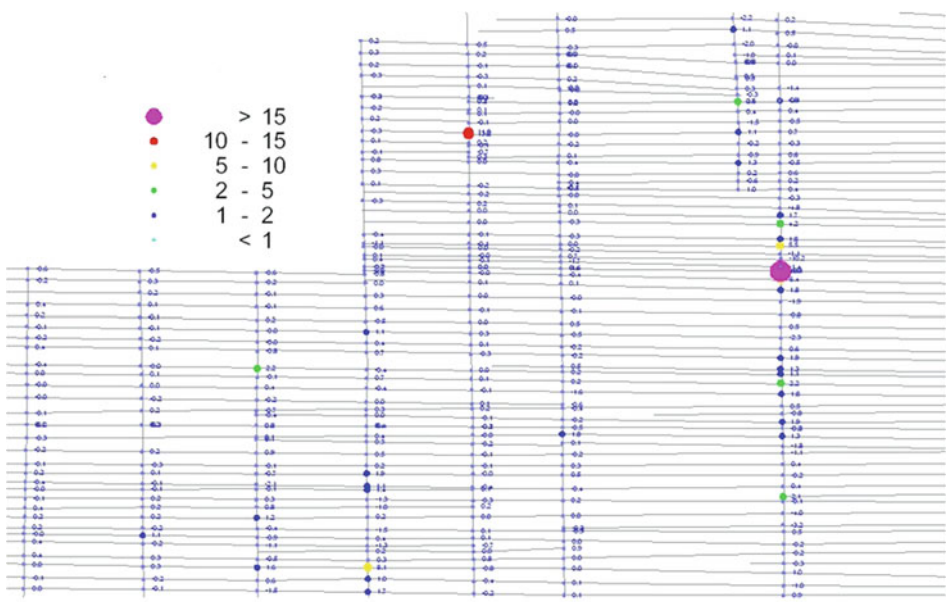

Fig. 4.7 Example of Tie-line cross-differences from an aeromagnetic survey over the Hoggar shield (Algeria). Radii of the colored circles are proportional to the difference in nT of the field

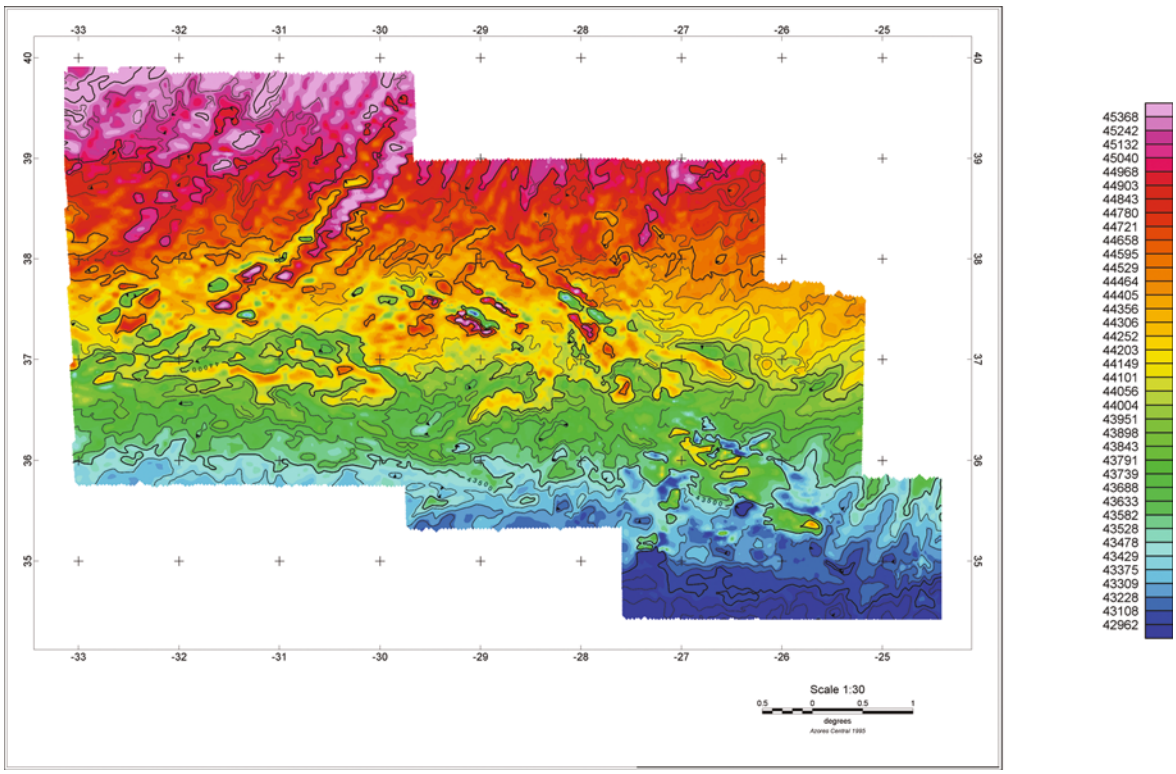

Fig. 4.8 Total field over the Azores Islands derived from aeromagnetic data (Luis and Miranda 2008). Color scale and contour lines are in nT

4.9 Lithospheric Field Mapping – Reference Field Correction

Depending on the time scale, the lithospheric or crustal anomaly field $\mathbf{B_a}$ is considered as a static field. Its characteristic wavelength ranges in from 10^{-5} km to 10^3 km. Its amplitude varies from few nT to some 10^3 nT at the Earth's surface. In some peculiar places, it reached 10^5nT and sometimes even larger than the main field (Heiland 1940; Logachev 1947). We may however assume that in general $|\mathbf{B_a}| \ll |\mathbf{B_N}|$ where $\mathbf{B_N}$ is the core field. It is also assumed that the orientation of the core field is almost uniform in the domain D. If this is not true, then the survey area can be divided into pieces small enough for the assumption to hold. Generally, for anomaly field mapping, only static fields are considered. The time duration of aeromagnetic surveying is usually short. In exceptional cases, they last long enough such that the data should be corrected for the secular variation of the main field (Luis 1996; Luis and Miranda 2008). If the external field is removed the Eq. (4.6) becomes:

$$\mathbf{B_t}(P) = \mathbf{B_N}(P) + \mathbf{B_a}(P) \tag{4.14}$$

Let us denote by $\mathbf{p}$ the unit vector in the core field direction, i.e.,:

$$\mathbf{p} = \frac{\mathbf{B_N}}{|\mathbf{B_N}|} \tag{4.15}$$

For airborne and marine magnetic surveys for which the magnitude of the field is usually measured, the total-field anomaly is defined as:

$$\Delta B = |\mathbf{B_t}(P)| - |\mathbf{B_N}(\mathbf{P})| \tag{4.16}$$

Bearing in mind that $\Delta B(P) \neq |\mathbf{B_a}|$, and under the assumptions given above, it is easy to show that:

$$\Delta B(P) \approx \mathbf{B_a}(P) \cdot \mathbf{p} \tag{4.17}$$

which is the projection of the field $\mathbf{B_a}$ onto $\mathbf{B_N}$. If ϕ is the angle between the two vectors, the error in

the approximation (4.17) is proportional to $B_N \sin^2 \phi$ The total field B_t derived ultimately using the leveling process contains contributions from sources of deep origin – i.e., in the core – and contributions from sources of shallow origin – i.e., in the crust. For geodynamic studies or for oil/mineral exploration purposes we are mainly interested by the crustal magnetic field. It is then very important to try to accurately characterize the normal field B_N in order to derive the anomaly field B_a or more precisely its approximation everywhere over the area of interest. Nowadays, the most widely used reference fields are the International Geomagnetic Reference Field (IGRF) or its "definitive" version (DGRF) (Barton 1997), the BGS Global Magnetic Model (BGGM) in the oil industry, and other global models such as CM4 (Sabaka et al. 2002, Sabaka et al. 2004). An IGRF-like model is a mathematical expansion of the Earth's main magnetic field using spherical harmonics basis functions (Chapman and Bartels 1940) up to a given wavelength. Before the Magsat era (Langel 1982), the accuracy of such models was of the order of 100–200 nT at the Earth's surface. Starting from 1980 with Magsat scalar and vector data the accuracy achieved was of the order of 20 nT at the Earth's surface. The Danish initiative Oersted and the German CHAMP geomagnetic satellites orbiting the Earth since 1999 and 2000 respectively, make it possible to achieve global field models with an unprecedentedly high accuracy of 10 nT (Olsen 2002; Olsen et al. 2009; Lesur et al. 2008; Lesur et al. 2009; Maus et al. 2005, 2009).

The IGRF/DGRF models describe not only the static part of the geomagnetic field up to degree and order 13 but also its secular variation up to degree and order 8. These models are updated every 5 years. Following the IAGA-Division V announcement for global field models, the present IGRF model, with an extrapolation valid for the 2010–2015 time interval, is the 11th generation (Finlay et al. 2010). The Gauss coefficients of the IGRF/DGRF models are available from year 1900 through 2010 (Barton 1997; Macmillan et al. 2003; Macmillan and Maus 2005; Finlay et al. 2010). The DGRF models are very useful for gridding or assembling adjacent aeromagnetic surveys flown at different epochs (Hemant et al. 2007; Hamoudi et al. 2007; Maus et al. 2007). They allow the earliest surveys reduced with inaccurate old versions of the IGRF models and to be used by correcting them for a new common reference field epoch. Most industrial potential field softwares include the IGRF as the main field model. For many of the earliest surveys, even in the early 1970's, an arbitrary and often unspecified constant was subtracted from the measured data before contouring the residual field. It often happens that the original data are no longer available. In that case, the derived grids may not easily be incorporated in any compilation such as the World Digital Magnetic Anomaly Map (WDMAM) (Hamoudi et al. 2007, Maus et al. 2007). To correct and merge inconsistent or discontinuous grids, accounting for the secular variation of the field for different epochs, the comprehensive model CM4 (Sabaka et al. 2002, Sabaka et al. 2004) is probably more efficient than the IGRF models (Hamoudi et al. 2007). For surveys of limited geographic extent, derivation of a local polynomial expression for the normal field is certainly a better approach than global modeling one to improve the definition, resolution and the accuracy of the anomaly field (Le Mouël 1969; Luis 1996; Chiappini et al. 2000, Supper et al. 2004). Second or third order polynomials better constrain the spatial gradients of the normal field than IGRF does and accurately represent the long wavelength components of this field. The analytical expressions may be derived either using (x, y) Cartesian coordinates or longitude (λ) and latitude (ϕ) geographic coordinates. In the former case the general expression for the normal field is then given by:

$$B_N(x, y) = \sum_{i,j} a_{ij} \Delta x^i \Delta y^j \tag{4.18}$$

The indices (i, j) give the degree of the polynomial expansion, generally of maximum order less than or equal to three. The coefficients are calculated from the measured data by least-squares. The necessary condition to use such a method is that the anomaly field has zero-mean over the area of interest (Le Mouël 1969) and that there are no magnetic sources outside the survey area. As an example of using longitude and latitude geographic coordinates, Chiappini et al. (2000) used a second order polynomial for the magnetic anomaly map over Italy and surrounding marine areas of the form:

$$\begin{aligned} B_N(\phi, \lambda) = {} & a_{00} + a_{10} \Delta\phi + a_{01} \Delta\lambda + a_{11} \Delta\phi \Delta\lambda \\ & + a_{20} \Delta\phi^2 + a_{02} \Delta\lambda^2 \end{aligned} \tag{4.19}$$

Table 4.2 Numerical expression of the 2nd order polynomial over Italy and surrounding marine areas (Chiappini et al. 2000)

Coefficients	Values	Unit
a_00	45386.500	nT
a_10	342.10	nT degree^{-1}
a_01	69.034	nT degree^{-1}
a_11	−1.868	nT degree^{-2}
a_20	−4.438	nT degree^{-2}
a_02	1.457	nT degree^{-2}

where: $\Delta\phi = \phi - \phi_0$ and $\Delta\lambda = \lambda - \lambda_0$ with ($\phi_0 = 42°N, \lambda_0 = 12°E$) being the latitude-longitude of the central point of the survey area . The coefficients $a_{ij}(i = 1, 2, j = 1, 2)$ are listed in Table 4.2.

As an example of Cartesian expression of the normal field, the coefficients of the second order polynomial expression based on the UTM26 projection system derived for the aeromagnetic survey of the Azores islands by Luis (1996), using Equation (4.18) to degree 2 in both i and j are given in Table 4.3. In this case

$$\Delta x = x - x_0 \tag{4.20}$$

and

$$\Delta y = y - y_0 \tag{4.21}$$

with $(x_0 = 420, y_0 = 4250)$ are the UTM coordinates of the central point of the survey expressed in kilometers.

Table 4.3 Numerical expression of the 2nd order polynomial over Azores Islands (Luis 1996)

Coefficients	Values	Unit
a_00	44184.0	nT
a_10	1.087	nT km^{-1}
a_01	4.215	nT km^{-1}
a_11	-0.66710^{-3}	nT km^{-2}
a_20	-0.11410^{-3}	nT km^{-2}
a_02	-0.74310^{-3}	nT km^{-2}

Figure 4.9 shows the differences in the magnetic field between the IGRF90 model and the local second order polynomial approximation over the Azores Islands. These differences range between −100 and −20 nT inside the survey areas, the magnitude of the global IGRF90 derived field is smaller than the magnitude of field derived using local polynomial expression. We can also see clearly that the map is mainly dominated by the long wavelength of the IGRF field and that its gradient is poorly constrained.

Figure 4.10 presents the anomaly of the total field calculated using (4.12) as an example. Even if the field measurements are very accurate, say with less than 1 nT Root-Mean-Square (RMS) noise, the anomaly field accuracy and its precision is often dependent on the positioning system used. With old positioning systems, 10–20 nT accuracy was commonly reached

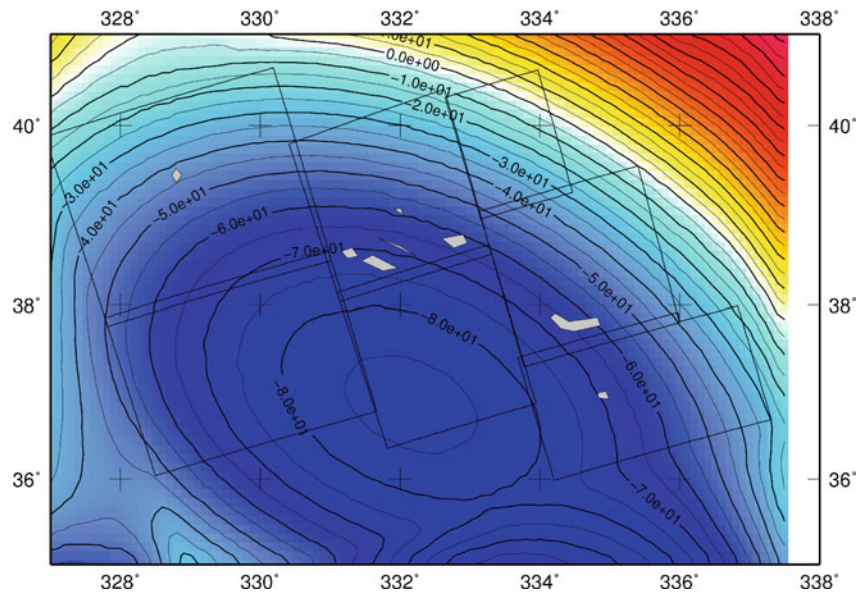

Fig. 4.9 Differences between IGRF90 and polynomial total fields over the Azores Islands (*grey polygons*). The seven aeromagnetic panels surveyed are shown by black rectangles. (Luis 1996)

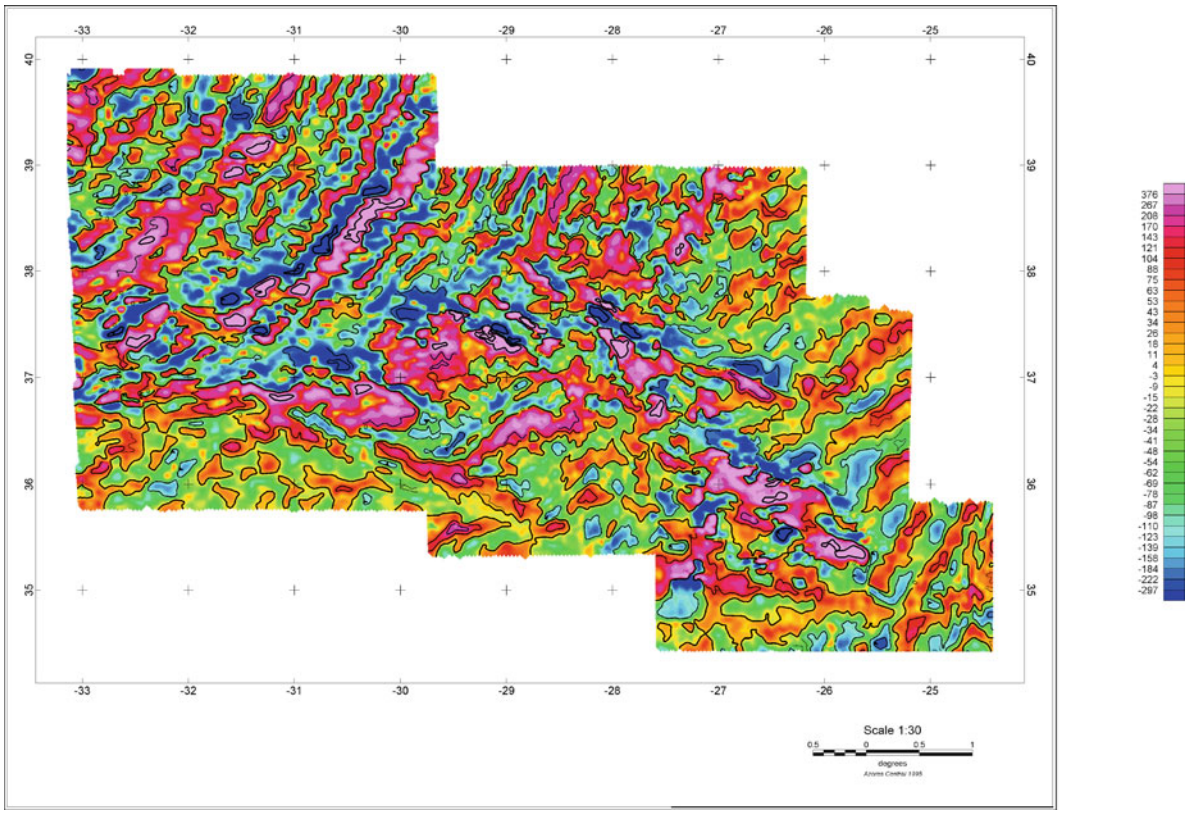

Fig. 4.10 Total field anomaly over the Azores islands derived from the aeromagnetic data. Color-scale and contour lines are in nT. (Data courtesy of J. Luis)

for the final maps. Nowadays, GPS (or dGPS), very high instrumental resolution of the order of a picoTesla and high frequency sampling rates up to ∼1 kHz measurements are standard (Nabighian et al. 2005). This significantly reduces the noise affecting the anomaly field, allowing mapping of the magnetic heterogeneities with unprecedented high precision. Such surveys prove to be useful even in a sedimentary context where the magnetic signal is very weak.

4.10 Further Processing: Micro-leveling

Image processing and data enhancement of the aeromagnetic anomaly maps shed light on leveling errors still contaminating the reduced data (Minty 1991; Paterson and Reeves 1985). Once contoured, the anomaly field may appear as fully leveled. However, graphic shading representation of the field shows not only small-scale geologic features as expected but also short wavelength low amplitude oscillations oriented along the flight lines. Such organized noise has been called "corrugations" and its removal is called de-corrugation (Paterson and Reeves 1985) or micro-leveling (Minty 1991). Fig. 4.11a below shows the aeromagnetic anomaly field data above the Tindouf basin in southwest Algeria (Allek 2005). The flight-line azimuth is N160°. We can easily see high frequency noise oriented along the flight-lines. Fig. 4.11b presents the same anomaly field after micro-leveling.

Micro-leveling remains an empirical filtering process. Its principle – it is purely numerical with no underlying physics – is described by Minty (1991). It may be applied to any measured quantity, not just potential field data. An example would be radiometric data. As with classical tie-line leveling, many algorithms have been developed and are used for micro-leveling. However, great care should be taken when filtering the noise to preserve geologic features with the same properties (i.e., main direction and spectral content) as the noise (Fig. 4.12).

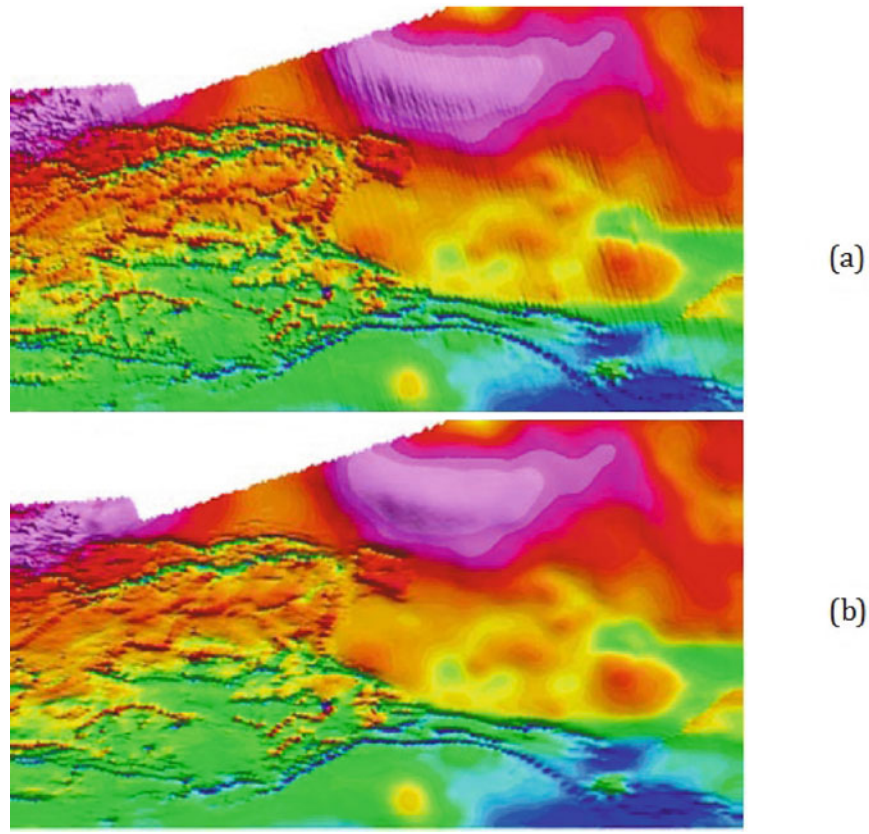

Fig. 4.11 Aeromagnetic anomaly field in the southwest of Algeria. Azimuth of flight-lines is N160°. (**a**) Before micro-leveling. (**b**) After micro-leveling (Allek 2005)

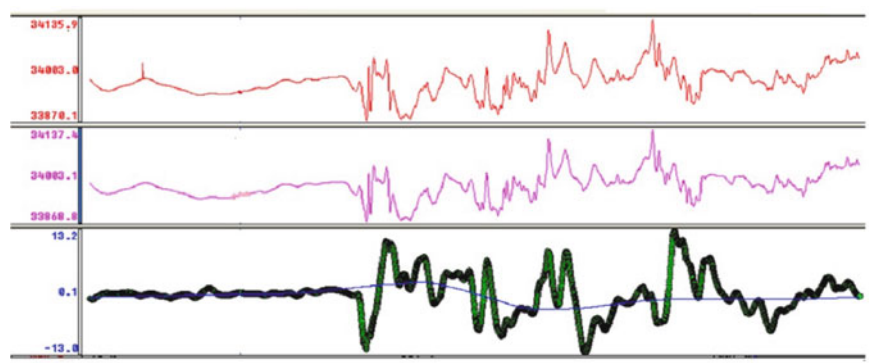

Fig. 4.12 Micro-leveling process. (*Top*) Raw aeromagnetic profile (*red*). (*Middle*) Micro-leveled profile (*pink*). (*Bottom*): High frequency error (*green*) and its smooth version (*blue*)

4.11 Interpolating, Contouring and Gridding

The anomaly of the total field, when all the errors have been corrected, can be interpolated and gridded. Various methods have been developed since the end of the sixties for automated contouring (Bhattacharyya 1969, 1971, O'Connell et al. 2005). The most popular and easy to use technique is probably the minimum curvature interpolation algorithm (Briggs 1974). Many sophisticated algorithms have been developed using kriging (Hansen 1993), fractal approaches (Keating 1993) or wavelets (Ridsdill-Smith and Dentith 1999). All these methods are proposed to alleviate the aliasing problem that may occur because the density of data is always so much greater along the flight-line direction than across flight lines. To cope specifically with this problem of different data density along and across

flight lines, bi-directional gridding was developped (O'Connell et al. 2005; Reford 2006).

The final gridded data are then ready to be plotted at scales, ranging from at least 1 : 250,000 to less than 1 : 5,000, and/or further processed in the space or spectral domains for geologic interpretation.

4.12 Conclusions for Aeromagnetics

Almost a century has passed between the first attempt in 1910 to measure the geomagnetic field from the air in a captive balloon and nowadays using unmanned aircraft vehicles. Many millions of line kilometres have been flown by governmental agencies, companies, and academic institutions throughout the world. Many kinds of magnetometers have been used: Earth's inductor, fluxgate, proton precession, Overhauser, optically pumped alkali vapour and SQUID magnetometers. Scalar and vector measurements have been collected onboard fixed-wing aircrafts, helicopters and very recently with unmanned vehicles. At a lesser extent stratospheric balloons have also been used for geomagnetic field measurements. The accuracy of measurements evolved over a very wide range from mT in 1930s to some fT nowadays. The positioning uncertainties improved by several orders of magnitude for horizontal distances, from hundreds of meters with tracking by cameras and video recovery systems to less than a centimetre in carrier-phase dGPS. The high-resolution aeromagnetic method is not only useful in mineral and oil exploration but also for cultural research of ancient archaeological sites and military purposes such as unexploded ordnance (UXO), and submarine detection. For safety reasons the actual tendency for "lower and lower altitude" is a strong argument in favour of UAV development. Future directions in UAV research would be towards stretching the boundary of autonomous operation through an efficient trajectory generation and mission planning. The development of small inexpensive UAV will allow a flexible and robust distributed sensor network to replace limited manned flights or large UAV that concentrate expensive sensor and communication systems in a single agent with a large team of operators. Two kinds of UAV are foreseen: stratospheric high altitudes UAV for regional surveys and low altitudes high resolution UAV. They will contribute by better describing the broad spectrum of lithospheric field magnetic anomalies. Regional airborne and shipborne surveys cover a significant part of the Earth's surface. However, large parts remain still unsurveyed. Despite the large disparities between surveys, the compilation of huge amounts of released data – of the order of 5×10^{12} data points – collected over many decades has allowed the derivation the first global anomaly map at the Earth's surface within the framework of the World Digital Magnetic Anomaly Map project (Korhonen et al. 2007). In aeromagnetic surveying, in the same way that gradiometer data have been shown to be superior to single sensor data, it is expected that acquiring vector data will give more information about geologic structures and their physical properties than can be obtained using scalar measurements only. Efforts have also to be made to improve the geological interpretation of the magnetic anomaly field with respect to the petrology of rocks. These studies will have a substantial overlap with current initiatives that address the fields from rock and mineral physics to lithosphere and deep continental drilling.

4.13 Introduction to Marine Magnetics

About 70% of the Earth's surface is covered by water. Aeromagnetic surveys can only help to study the regional magnetic signal of the lithosphere over the oceans close to continents (e.g., Blakely et al. 1973, Malahoff 1982) or in remote oceanic areas with long-range high-altitude surveys like Project Magnet flights, whereas satellites also fly over the oceans but provide low resolution measurements. Therefore marine magnetic observations, defined here as magnetic measurements along ship tracks or from underwater autonomous vehicles, are the only way to study the magnetic signal over the oceans and seas at local and regional scales. This magnetic signal is due to the induced and remanent magnetization carried by the oceanic crust and uppermost lithosphere. For instance, when newly-formed crust cools at mid-oceanic ridges, it acquires a thermoremanent magnetization which 'freezes' the ambient magnetic field; the uneven sequence of geomagnetic field reversals recorded by the oceanic crust represents the best geophysical witness of lithospheric plate motions (Vine and Matthews 1963). This shows how crucial

are the marine magnetic observations. Forward and inverse modeling approaches have been applied to retrieve the magnetic properties of the Earth's oceanic lithosphere (e.g., Parker and Huestis 1974; Schouten and Denham 1979; Pariso et al. 1996; Langel and Hinze 1998; Sichler and Hékinian 2002; Purucker and Whaler 2007). Apart from their obvious interests for marine geophysics and geology, other applications are nautical archaeology (e.g., Boyce et al. 2004; Van Den Bossche et al. 2004) as well as ocean engineering (i.e., pipeline or undersea cable detection). The few magnetic field observations for the latter two topics are not considered in this review study.

Acquiring magnetic measurements onboard a ship is not a straightforward task. First, compared to the planes used in aeromagnetics, oceanographic vessels are slow, implying less regional mapping capacity. Second, the magnetization of ships is usually very high, a problem solved by towing the magnetometer (at least) several hundred meters astern (and in some cases below) the ship – with less control on the sensor position and attitude. Third, the survey areas are usually quite remote from any magnetic observatory, making it difficult to estimate and subtract external field contributions from the Total-Field (TF) observations.

Magnetic measurements for scientific purposes really started in the 1950s. Indeed the submarine or mine detection during the Second World War and the Cold War triggered technological developments which considerably increased the accuracy of magnetometers. By 2010, all oceans had been covered by marine magnetic measurements, with gaps in the Southern Hemisphere. Such observations are made in most marine geophysical surveys with interests in the oceanic crust.

In the following sections, we present some general aspects of marine magnetic measurements. The first part concerns the global history of standard (scalar) observations from a statistical point of view and their main applications. The second part focuses on the typical sources of error when acquiring these data, and shows how to improve the quality of scalar marine datasets. The last part deals with peculiar instruments allowing vector and/or deep sea measurements and the corresponding processing techniques.

4.14 History of Marine Magnetics

4.14.1 The First Attempts

The first magnetic measurements at sea may have been made by a Chinese sailor with a compass onboard a ship about 2000 years ago. However, without any written reference to such an hypothetical event, we should attribute the first record of magnetic measurements at sea, in this case declination determinations, to Portuguese navigators. Merrill and MeElhinny (1983) mention that, in 1538–1541, João de Castro used a compass like a sun-dial with a magnetic needle to determine the azimuth of the sun at equal altitudes before and after noon. The half difference of these azimuths measured clockwise and anticlockwise respectively was the magnetic declination. He performed about 43 declination measurements when he commanded a ship that sailed to India and in the Red Sea. About a century and half later, in 1702, many similar observations led to the first declination chart of the whole Earth, published by Edmond Halley. Over two centuries more were needed to develop magnetic field theory (Gauss) and the first portable magnetometers.

Allan (1969) reports that a non-magnetic research ship named 'Carnegie' sailed between 1909 and 1929 and made magnetic measurements along widely spaced tracks in the Atlantic, Pacific and Indian oceans. During the Second World War, magnetometry at sea was used to detect submarines and mines (Germain-Jones 1957). The fluxgate magnetometer, originally developed as an airborne instrument for the detection of submarines, was converted for marine research at Lamont Geological Observatory (Allan 1969). The first measurements made with such a magnetometer towed behind a ship were reported by Heezen et al. (1953). Subsequently, the fluxgate magnetometer was largely superseded by the proton magnetometer, because the latter gives an absolute measurement of the field. Packard and Varian (1954) first developed this instrument, which was later adapted for land use by Waters and Phillips (1956) and modified for towing behind a ship by Hill (1959). Finally, in the late 1950s, the Scripps Institute of Oceanography and the United States Coast and Geodetic Survey made a detailed magnetic survey over a large area off the west coast of the United States (Mason 1958; Mason

and Raff 1961; Raff and Mason 1961; Vacquier et al. 1961), opening the way for many marine magnetic surveys worldwide.

4.14.2 Evolution of the Global Dataset

Once the proton precession magnetometer became the standard instrument to measure the magnetic field over marine areas, oil and gas companies – who already used magnetic land prospection to help detect reservoirs – deemed marine magnetic surveys a complementary technique to reflection seismic. Although only a few public reports of marine magnetic prospection for oil and gas exploration are available, such exploration helped to spread the use of magnetometers at sea.

Figure 4.13 shows the evolution of the annual number of marine magnetic surveys over the world's oceans. These values are mainly extracted from the databases of Quesnel et al. (2009) and GEOphysical DAta System (GEODAS). The reader must be aware that many magnetic surveys carried out by private companies or by scientific institutes that did not share information on their data were not taken into account. The main trends should remain similar if these missing data were added. The values should be updated for the years since 2002: cruises in 2003–2010 will probably be released to the databases after 2010.

The histogram highlights how the number of cruises increased during the 1960s and 1970s, with a peak in 1972. Following Vine and Matthews (1963), these years mark the recognition of Plate Tectonics as the new paradigm for Earth Sciences, leading to an unprecedented effort of new marine data collection to validate the concept and derive first-order models of present and past global plate kinematics. Magnetic measurements were made routinely during most cruises and transits. Remarkably, the steady increase in number of surveys – hence in budgets allocated to these surveys – breaks in 1973, the year of a major international oil crisis.

Since the end of the 1970s, the annual amount of marine magnetic surveys has decreased regularly (Fig. 4.13), except for a small rebound in the late 1980s. Although many regional and local problems remain unsolved, plate kinematics is seen as understood at the first order, and the reduction of

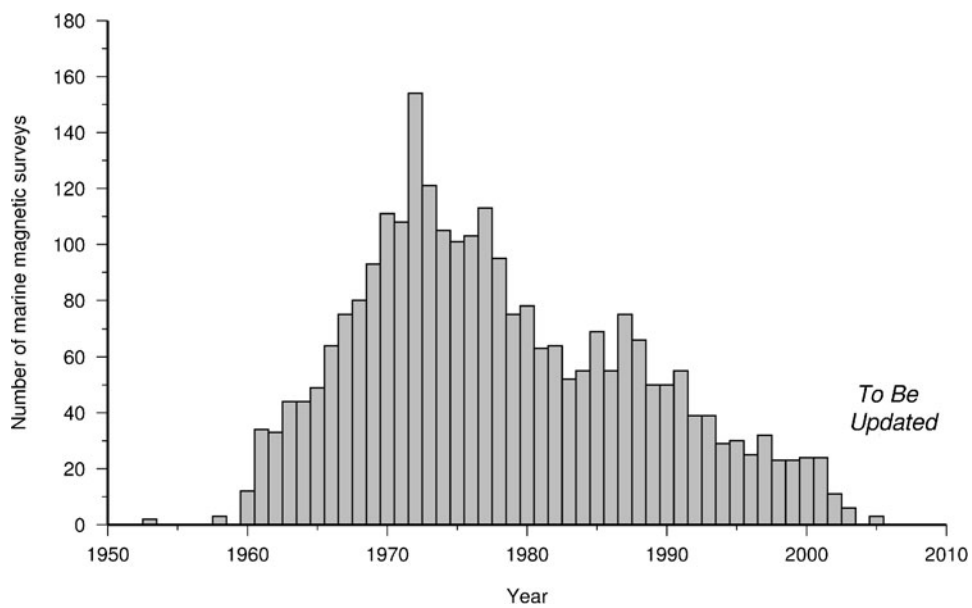

Fig. 4.13 Annual frequency of marine magnetic surveys since 1950. Most of these campaigns are stored at the GEODAS database. For years after 2002 the number of stored cruises is not fully updated

budgets led to the acquisition of magnetic measurements as a secondary consideration. Nowadays, only ~20 scientific cruises acquire magnetic measurements each year. Until recently, these cruises were noticeably supported by international scientific programs such as the International Ocean Drilling Program (IODP) – formerly the Deep-Sea Drilling Program (DSDP) and Ocean Drilling Program (ODP). Unfortunately, IODP recently decided to stop the systematic acquisition of marine magnetic measurements during their transits for budgetary reasons. Furthermore, the enforcement of Exclusive Economic Zones (EEZ) 200 nm (nautical miles) away from the coastal states and their future extension up to 300 nm under the UNCLOS (United Nation Convention for the Law Of the Sea) adds the difficulty of obtaining official permission to acquire data in these EEZ through the diplomatic channels, with 6 months notice.

Figure 4.14 represents the same data as Fig. 4.13 split into the Pacific, Atlantic and Indian oceans (left), or the Northern and Southern Hemispheres (right). Again, numbers for the recent years are probably underestimated. The Indian Ocean always had fewer cruises than the other oceans, partly because of its reduced size, and partly because of its remote location from the United States (US), Japan and Europe. The former Soviet Union collected numerous cruises over the Carlsberg Ridge (see, e.g., Merkouriev and DeMets 2006, and references therein), but these data are not considered in this study. In contrast, the northern Pacific Ocean was extensively investigated by US and Japanese research vessels. The Southern Hemisphere

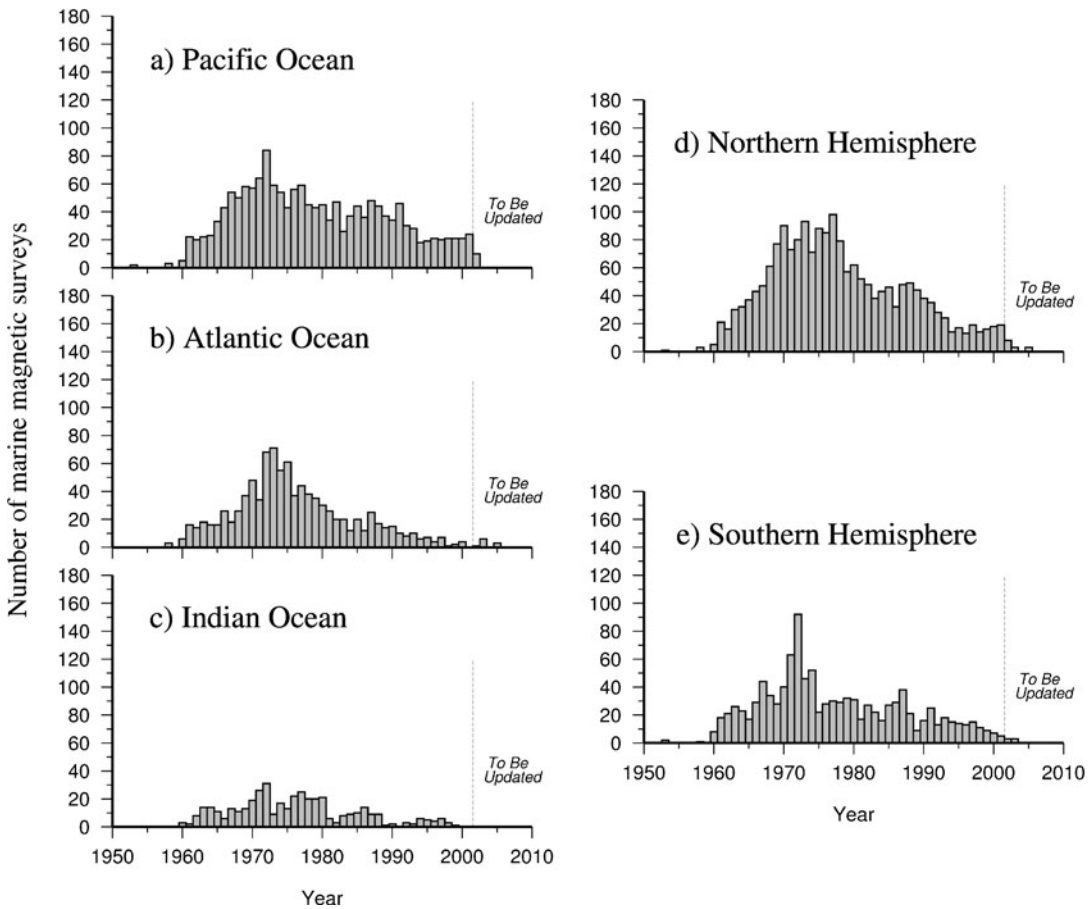

Fig. 4.14 Same as for Fig. 4.13, but only for surveys in the (**a**) Pacific Ocean, (**b**) Atlantic Ocean, (**c**) Indian Ocean, (**d**) Northern Hemisphere and (**e**) Southern Hemisphere. Note that these histograms could be biased by surveys belonging to two (or more) parts, but this should not greatly affect the main tendancies

was always much less explored by marine magnetic surveys than the Northern, except in 1972 when both hemispheres reached the same level.

Figure 4.15 shows the spatial evolution of the marine magnetic coverage from the first cruises before 1960 to the present. Vessels towing a magnetometer had already reached the mid-Pacific and mid-Indian oceans by 1960. A big transition occured in the 1960s (as Fig. 4.13 has already shown), when only the South Indian and South Atlantic oceans remained poorly covered by magnetics. Between 1970 and 1980, these gaps were partially filled. Since 1980, marine magnetic data coverage has not changed much, except the highest concentration in the Pacific Ocean near Antarctica. Areas close to the continents exhibit a lot of marine magnetic measurements. The final panel of Fig. 4.15 reveals a remaining dichotomy between the well-covered northern parts of the Pacific, Indian and Atlantic oceans versus their southern counterparts. It is obvious that further marine magnetic acquisition is needed for Antarctica and sub-Antarctic waters as well as for the Arctic Ocean (even if aeromagnetic data, not included in Fig. 4.15, exist in these areas). The dataset used to build this map (see end of Section 4.14.3) will be complemented by additional analog data (to be digitized) and some other cruises unavailable to Quesnel et al. (2009) to prepare an updated version of the marine magnetic dataset to be included in the next World Digital Magnetic Anomaly Map (WMAM; Korhonen et al. 2007, and T. Ishihara, pers. comm.).

4.14.3 Storage and Accessibility

A substantial fraction of the world marine magnetic observations from 1953 to present are available in digital format from the GEODAS database[1] hosted by the National Geophysical Data Center (NGDC). Some data are also stored by GEODAS in analog format as scanned documents. They appear mostly as handwritten charts where exact values of measurements plus time and space positioning are difficult to read. Some digital data were digitized from reports, a transfer resulting in additionnal errors.

[1] http://www.ngdc.noaa.gov/mgg/gdas/

Among the numerous research institutions which carried out marine magnetic surveys stored in the GEODAS database, the United States takes the lead with the Scripps Institute of Oceanography (over 550 cruises), the Lamont-Doherty Earth Observatory (over 540 cruises), the US Navy (about 130 cruises), the United States Geological Survey (USGS, about 120 cruises), the Woods Hole Oceanographic Institute (about 110 cruises), as well as universities like the University of Hawaii (about 130 cruises). Many other marine magnetic cruises were provided by Japanese institutions like the Japan Hydrographic and Oceanographic Department (JHOD; over 200 cruises) or the Geological Survey of Japan (about 40 cruises). France (about 180 cruises with about 50% from Ifremer), New Zealand (about 100 cruises), the United Kingdom (about 90 cruises), Australia (about 70) and South Africa (about 20 cruises) also contributed marine magnetic observations to the data base.

A few other databases storing marine magnetics exist. Some include cruises stored at NGDC, some not. Such databases belong to national and international research institutes, sometimes to specific laboratories. Free access to the data is usually straightforward for *bona fide* scientists for research purposes. Table 4.4 gives a non-exhaustive list of geophysical databases where marine magnetic observations are available. This table, and particularly internet URLs, are valid in 2010 and may change in the future.

Additionally, Germany performed numerous surveys (over 100; U. Barckhausen, pers. comm.) and contributed to world marine magnetic coverage. Similarly, the former Soviet Union (and later Russia) collected a large amount of data through systematic regional surveys undertaken, for example, in the North Atlantic and the Northwestern Indian oceans, amounting to about 2–3 millions of kilometers (S. Merkouriev, pers. comm.). Some of these data have been used by Verhoef et al. (1996), Merkouriev and DeMets (2006) and Merkouriev and DeMets (2008).

4.14.4 Scientific Objectives

Apart from oil and gas prospection (for which magnetics plays only a secondary role), the main application of marine magnetics is the study of the Earth's oceanic

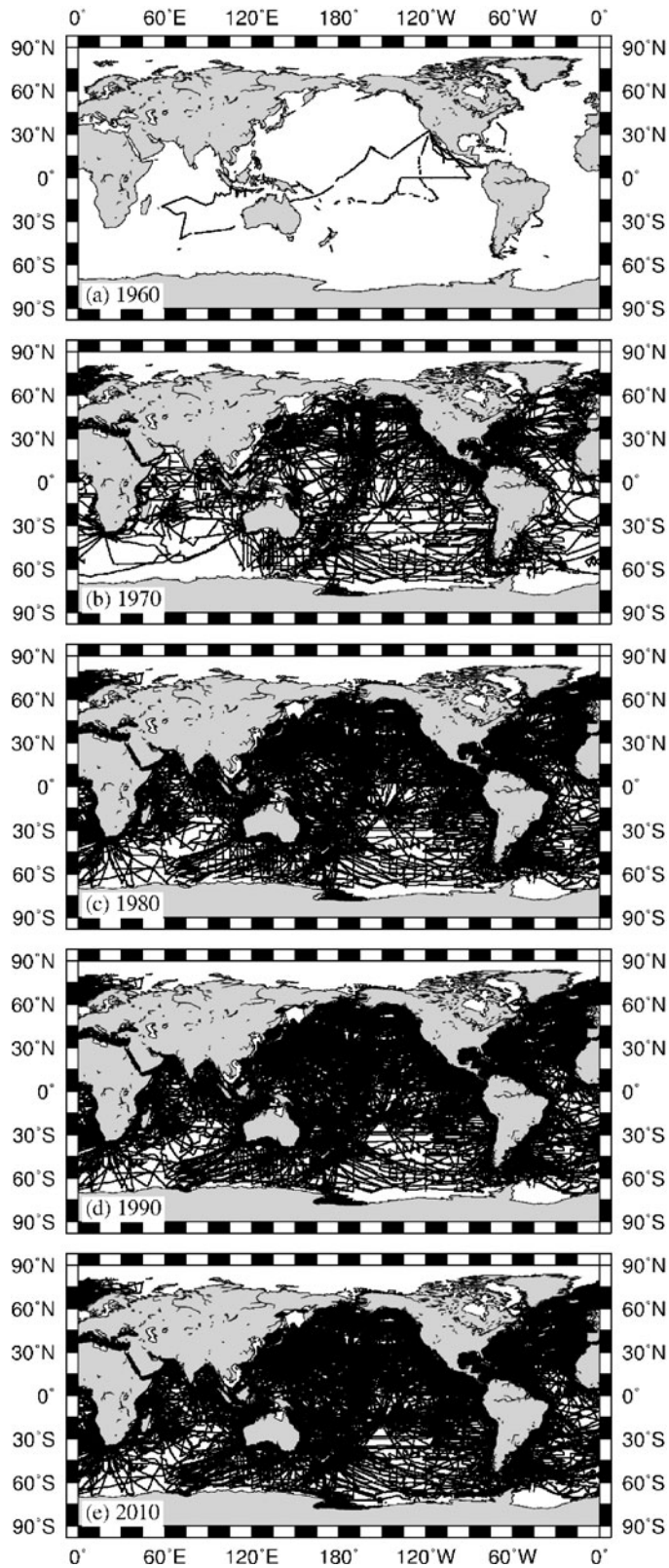

Fig. 4.15 Global marine magnetic survey coverage in (**a**) 1960, (**b**) 1970, (**c**) 1980, (**d**) 1990 and (**e**) 2010

Table 4.4 Databases with marine magnetic observations

Name/Acronym[a]	Institute[b]	URL (in 2010)
GEODAS	NGDC	http://www.ngdc.noaa.gov/mgg/gdas/
SISMER	IFREMER	http://www.ifremer.fr/sismer/
BAS	BAS/NERC	http://www.antarctica.ac.uk/bas_research/data/
JODC	JHOD JCG	http://www.jodc.go.jp/NEW_JDOSS_HP/MGD77_info_e.html
JAMSTEC	JAMSTEC	http://www.jamstec.go.jp/dataportal/
SeaDOG	NOC/NERC	http://www.noc.soton.ac.uk/cgibin/seadog/

[a]Acronyms are: GEODAS, GEOphysical DAta System; BAS, British Antarctic Survey; JODC, Japan Oceanographic Data Center; JAMSTEC, Japan Agency for Marine-Earth Science and Technology; SeaDOG, Sea Deep Ocean Geophysical data.
[b]NGDC, National Geophysical Data Center; IFREMER, Institut Francais de Recherche pour l'Exploitation de la Mer; JHOD, Japan Hydrographic and Oceanographic Department; JCG, Japan Coast Guard; NOC, National Oceanography Center; NERC, Natural Environment Research Council.

crust and uppermost mantle through its magnetization at all scales in time and space. Their contribution is essential to constrain the structure, age and evolution of ocean basins, from ridge to subduction. Other applications include constraints on the magnetic structure and properties of passive and active margins, mid-oceanic ridges, transform faults, subduction zones, seamounts, and fracture zones. Such constraints have implications for the geologic processes which affect or affected such areas. At smaller scales, archaeological prospection sometimes requires magnetic measurements to detect submerged constructions or sunken vessels.

4.15 Sources of Error, Evolution and Correction for Scalar Sea-Surface Measurements

This section describes the different problems associated with marine magnetic observations, from the acquisition to the storage, and the possible method of minimizing the resulting errors on the data. Further details can be found in Jones (1999) and Quesnel et al. (2009).

4.15.1 Magnetic Observation Accuracy

Magnetometers and sampling rates evolved since the first measurements. Here we show how this evolution reduced the systematic errors associated with marine magnetic data acquisition.

4.15.1.1 Definitions

Some common terms concerning magnetometers used at sea need to be defined. Most of the following definitions are well-described in Hrvoic (2007).

The **resolution** of a magnetometer corresponds to the minimum variation of the magnetic signal (in nT) that the measurement device (not the sensors) can detect. Conversely, the **sensitivity** reflects the minimum signal variation that the whole instrument can detect. It depends on the sensor noise level and is often represented in units of $(\mathrm{nT}(\sqrt{\mathrm{Hz}})^{-1}$ since the sensor frequency bandwith will also influence this noise.

The **drift** denotes a small variation of the magnetometer output with time and eventually temperature without any real change of the ambient magnetic field external to the instrument. It mainly concerns the sensor itself, even if the electronics of the measurement device can also be affected by temperature changes. To determine the drift, one must calculate the noise spectrum in the frequency domain: if this spectrum is flat, then no drift will occur with time. The **heading error** corresponds to the small change of the magnetometer output related to a change of the magnetic field direction with respect to the sensor. It can be due to ferromagnetic electronics close to the sensor. Finally, the range of heading directions for which the sensor cannot acquire any measurements is called the **dead zone**.

The aim is to reduce the last three parameters, and the resulting total error is expressed as the **absolute accuracy** of the magnetometer.

4.15.1.2 Fluxgate Magnetometers

Fluxgate magnetometers (three sensors oriented at right angles) were used for early surveys. At this time, these instruments had an estimated accuracy of several nT (Bullard and Mason 1961). Errors were amplified by the low sampling rate, recorded (and sometimes manually handled) every 5–10 min (Quesnel et al. 2009) and sometimes by the small distance between the instrument and the ship. Both effects have to be taken into account when using these old surveys. Proton precession magnetometers were soon preferred, since the three fluxgate sensors have to be very accurately oriented with respect to each other (possible orthogonality errors) and since such vector sensors have a significant drift with time and temperature, therefore requiring calibration.

Nowadays, fluxgate magnetometers offer better than 0.1 nT $(\sqrt{\text{Hz}})^{-1}$ sensitivity, for about 0.01 nT of resolution. Their final accuracy depends on the gyro tables on which they are mounted (Nabighian et al. 2005). The use of fluxgate magnetometers at sea is presented in Section 4.16.

4.15.1.3 Proton Precession Magnetometers

Hill (1959) suggested using nuclear spin (later called proton precession) magnetometers onboard ships. These instruments have the advantage of having no drift and therefore not requiring frequent calibrations. At this time, an absolute error of several nanoTeslas was usual, whereas the accuracy of modern proton magnetometers reaches 0.1 nT (Sapunov et al. 2001). More typical values would be 0.1 nT at 0.2 Hz for portable instruments (Nabighian et al. 2005).

The sampling rate in early surveys was generally a measurement every 30 s at a ship's speed of 10 knots (Allan 1969), adequately suited to a proton-precession magnetometer cycling every 10 s at most. Because the proton precession signal cannot be sampled during the polarization in the sensor, this sampling rate could not be increased. Another limitation was that the polarization requires a lot of energy, transported to the instrument through a thick armoured coaxial cable. The measured signal is transported back to the ship in analog form through the same cable and is very sensitive to any electric noise generated by various devices on the ship. Furthermore, the proton precession magnetometers do not prevent erroneous measurements from rotations or small motions of the sensor head during acquisition ('dead zone'; see Section 4.15.1.1).

4.15.1.4 Optically-Pumped or Alkali-Vapor Sensors

Since they provide excellent sensitivity (less than 0.01 nT) and very high sampling rates (more than 10 Hz) for a light and compact instrument (Nabighian et al. 2005), alkali vapor magnetometers are suitable to achieve high quality magnetic observations at sea. However, the fragility of the glass envelope and an intrinsic heading error limits their use.

4.15.1.5 Overhauser Effect Sensors

The Overhauser magnetometer is a variation of the proton precession instrument, which it has superseded for the last 20 years (Hrvoic 2007). This instrument is now widely used for marine surveys. It requires lower power than standard proton precession magnetometers, provides a dramatically higher signal to noise ratio, and avoids shipboard noise sources and data 'line loss' associated with the transmission of weak analog voltages usually met with proton precession sensors. Since the sensor can be polarized in tandem with precession signal measurement (because of different frequency bandwidths), faster sampling rates are also possible (Hrvoic 2007). Typically, the field can be sampled at 5 Hz with a resolution of 0.01 nT to 0.001 nT for a sensitivity of 0.015 nT at 1 Hz (Anderson et al. 1999). It also delivers very high absolute accuracy (0.2 nT), eliminating drift, heading error, and orientation problems.

4.15.2 Ship Noise

Due to their composition and engines, ships typically devoted to scientific surveys are magnetic. To reduce their magnetic effect, the magnetometer is towed at large distance from the ship, a method initiated in the 1960s (Bullard and Mason 1961; Laughton et al. 1960). Care must therefore be exercised with data prior

to 1960. During GEODAS dataset analysis, Quesnel et al. (2009) nevertheless discovered small shifts of magnetic field mean level within many post-1960 cruises which were probably due to heading effects of the ship noise on the measurements. Indeed the ship's magnetism varies with the direction of the cruise (and so the orientation of the ship with regard to the sensor). It also evolves as the ship keeps a constant heading for some time, resulting in the acquisition of a viscous magnetization component. From theoretical work and experiments carried out at sea, Bullard and Mason (1961) estimated the effect of the ship on different headings in order to reduce the associated magnetic data. For instance, at the location of their experiment they found that a North-South survey will amplify this effect, whereas it is less than 1 nT at a distance of two times the ship length astern. At their time 1 nT was an acceptable error, but later surveys reached negligible values by towing the instrument at a greater distance. Nowadays, a cable 200 m-long or more is commonly used.

4.15.3 Position of the Ship

A very precise positioning measurement is needed for marine magnetic observations since the estimates of external and core magnetic field values (to be subtracted from TF measurements) vary spatially. The quality of positioning mainly depends on the date of the survey. Quesnel et al. (2009) also found obvious positioning errors in the GEODAS dataset such as cruises apparently located on land. Only comparison between adjacent and overlapping surveys can reveal the effect of such errors.

Accurate navigation in the open ocean was difficult in the past (Allan 1969). Field gradients of a few hundred nanoTeslas per km are not uncommon and the difficulty of matching up linear features from one area to another can be hazardous if ordinary 'dead-reckoning' navigation is used. Moored buoys fitted with radar reflectors were used to provide a reasonable relative accuracy in limited areas. The absolute position of a ship was believed known to within 100 m (Heirtzler 1964). The use of long-range radio navigation systems such as LORAN C or DECCA has improved the accuracy of magnetic surveys, where available (Allan 1969). At the end of the 1960s, the DOPPLER satellite navigation system, which combined a fixed accuracy of about 100 meters with world-wide coverage, brought greater precision to survey work (Talwani et al. 1966).

In the early 1990s, the Global Positioning System (GPS) appeared. At sea the error on position was initially less than 100 m (degraded mode), and was further reduced to less than 20 m in 2000. Therefore the towing distance must be determined as accurately as possible to properly differentiate the location of the ship and the measurement.

4.15.4 Date and Time of the Measurement

Errors in the acquisition time of marine magnetic measurements may affect the estimation of the external and core field (see Sections 4.15.6 and 4.15.7). However, even in the 1960s, the precision of clocks was acceptable to properly estimate these parameters at low and moderate sampling rates. Furthermore, higher sampling rates were later accompanied by higher precision of the time determination due to improvements in clock technology. Therefore such errors do not affect the quality of the computed magnetic anomaly values.

4.15.5 Transcription Errors

A valid measurement can be badly recorded. For early surveys (before magnetic tapes and, later, digital recording), manual data handling led to numerous erroneous values. Common errors are swaps of two digits of the total-field or resulting anomaly values (Quesnel et al. 2009). Therefore, one can not distinguish between an instrumental error and a transcription error. Along a track, such errors appear as spiky or shifted, isolated or grouped values that cannot be explained by commonly known sources of error.

Since such errors have very different amplitudes (10–100,000 nT) in the signal along track, it is difficult to assess their influence on the quality of a cruise. Quesnel et al. (2009) manually erased or corrected such erroneous data and/or applied filters to the noisy signal along-track. Finally, and after other kind of corrections, they were able to reduce the Root Mean Square (RMS) crossover differences (i.e., the difference between measurements at the intersection of two

ship tracks) of their global dataset from 180 nT to 82 nT. Then, they adjusted the long-wavelength signal of each track and used a specific line-leveling method to reduce inconsistencies between different surveys. The resulting RMS of crossover differences of their dataset was 36 nT, which improved the coherency of magnetic maps at sea whatever the anomaly wavelength (Quesnel et al. 2009). We would like to point out here that although the principle is similar, the aeromagnetic leveling procedure is much more efficient because the flight-lines and tie-lines are orthogonal and contemporaneous.

Most of the marine magnetic data are stored in data bases as raw total-field measurements and the associated anomaly values. The estimates of external and core magnetic field values used to derive the anomaly values are usually not stored (Quesnel et al. 2009). In the next two sections, we consider the errors generated by the calculation of total-field anomaly values, whatever the quality of the raw total-field measurements. Moreover, if the date, time or location is erroneous, then the estimates of external and core magnetic field values will be inadequate, resulting in a poor magnetic anomaly value.

4.15.6 Estimation of the External Magnetic Field

For early cruises, reference stations such as the nearest magnetic observatory were sometimes used to reduce the external magnetic field effects, whatever the distance from this observatory. It resulted in a very poor estimation of the external magnetic field, especially when the vessel sailed in remote oceanic areas. Some attempts were made by Laughton et al. (1960) to use the mean of noon measurements as the absolute external field contribution on all measurement of a survey. They also minimized the diurnal variation by performing measurements at night. Finally, they corrected their measurements by about 5 to 15 nT to remove the external field.

Despite this exception, almost all marine magnetic data stored in the data base up to the 1990s are not corrected from the external field. A recently derived method to correct such data is to use Comprehensive Models such as CM4 (Sabaka et al. 2004) to estimate the external field at every time and location for the last fifty years (Ravat et al. 2003).

4.15.7 Estimation of the Core Magnetic Field

The International Geomagnetic Reference Field (IGRF) models of the survey period are commonly used to remove the core field from the total-field measurements at sea. They consist of spherical harmonic coefficients that predict the main field and its secular variation over 5-year intervals (Macmillan and Maus 2005). These models are regularly revised to generate a Definitive Geomagnetic Reference Field (DGRF). Therefore magnetic anomaly data of adjacent surveys carried out at different times may have different values resulting from an imprecise estimation of the core field.

Again, the Comprehensive Models can be used to subtract the core field from the initial total-field measurements (Ravat et al. 2003; Quesnel et al 2009). For recent epochs (after 2002) for which no Comprehensive Model is available yet, other geomagnetic field models such as CHAOS or GRIMM have to be used (Olsen et al. 2006; Lesur et al. 2008).

4.15.8 Summary of Marine Magnetic Observation Errors

In Table 4.5, we summarize the different errors (expressed in nT) associated with marine magnetic observations and their evolution over the last 50 years, allowing the reader to be aware of the quality of the data.

4.16 Unusual Instruments and Processing Approaches

In this section, we first describe how vector marine magnetic observations became possible over the last thirty years. The second part is devoted to deep water measurements.

Table 4.5 Evolution of errors associated with marine magnetic data

Type	Old data	Recent data	Solutions
Sensor[a]	0.1–1 nT	0.001–0.01 nT	Overhauser effect sensors
Ship noise	>1 nT	negligible	Large towing distance
Ship position[b]	1–100 nT	<1 nT	Radio, Doppler and later GPS
Date and time[c]	negl.	negl.	Manual/visual check of datasets
Transcription[d]	1–10000 nT	negl.	Digital recording, check of datasets
External field estimation[e]	1–100 nT	∼1 nT	Mag. obs. data, CM4 or other models
Core field estimation[f]	10–100 nT	∼1 nT	Mag. obs. data, CM4 or other models
Total error	0.1–10000 nT	0.001-1 nT	Cleaning and leveling of datasets[g]

[a]depending on the type of sensor, but we can consider the proton precession system as the most widely used for magnetometers at sea; for fluxgate sensors, see Section 4.16.1.
[b]depending on the ambient magnetic anomaly gradient, and difficult to quantify for recent data since GPS should provide very precise positioning.
[c]time, and sometimes date, is missing in few trackline datasets that we should not consider except if we retrieve this information. A small error in acquisition time should not greatly affect the resulting magnetic anomaly (Quesnel et al. 2009).
[d]often swap of one digit in a total-field value transcription.
[e]most of the marine magnetic data were not corrected for external field variations until recently; Mag. Obs., Magnetic Observatory; CM4, Comprehensive Model 4 of Sabaka et al. (2004).
[f]depending on the first IGRF models for early surveys.
[g]see Quesnel et al. (2009).

4.16.1 Vector Marine Magnetic Observations

Nowadays, fluxgate magnetometers offer better than $0.1\,\mathrm{nT}(\sqrt{\mathrm{Hz}})^{-1}$ sensitivity, for about 0.01 nT of resolution. With such performance, it becomes possible to envisage the acquisition of vector magnetic measurements, i.e., the three components of the magnetic field, at sea. Such data would not substitute for absolute scalar measurements made with Overhauser magnetometers towed astern the ship. However, they may usefully complement these data. Indeed, the scalar magnetic anomaly of N-S trending structures near the Equator is almost zero, whereas the components of the vector anomalies still show some significant signal (Gee and Cande 2002; Engels et al. 2008). Furthermore, the three-component magnetic anomaly of elongated (2D) structures has the interesting property of having similar vertical and horizontal components, phase-shifted by $\frac{\pi}{2}$ (Isezaki 1986). Using this property, it is possible to estimate whether an anomaly is associated with a 2D or a 3D causative source, i.e., if the anomaly is a standard Vine and Matthews (1963) anomaly – an isochron of seafloor spreading, or a more complex structure such as a seamount or some kind of tectonic complexity. Furthermore, assuming that the anomaly is caused by an elongated (2D) body, it is possible to determine its orientation: it is the horizontal direction orthogonal to the vector anomaly, i.e., the direction along which the anomalous field is null. This ability to determine structural directions may be of importance in the case of single profiles or widely-spaced survey lines (such as those required for standard swath bathymetry), over sedimentary areas.

A major requirement to obtain accurate vector magnetic measurements is the knowledge of the sensor attitude, for instance by coupling the magnetic sensor to an inertial motion sensor. The final accuracy depends on that of the attitude sensor (Nabighian et al. 2005). Two types of instruments have been successfully tested: a towed vector magnetometer, in which both fluxgate magnetometer and inertial attitude sensors have been combined in a single 'fish' (Gee and Cande 2002; Engels et al. 2008) and Shipboard Three-Component Magnetometers (STCM), in which a three-component fluxgate magnetometer is installed on the ship's mast to take advantage of the ship's attitude sensor. Such a sensor is required for other instruments such as multibeam echosounders (e.g., Isezaki 1986; Seama et al. 1993; Korenaga 1995). The towed vector magnetometer has no specific correction for the vehicle magnetization: the only limitation is the high cost of any accurate attitude sensor, which one may hesitate to install in a towed (and easily lost) fish. Conversely, the STCM is affected by the strong magnetic effect

of the ship, which should be adequately modelled and removed. Installing the fluxgate sensors on a mast, the extreme point of the ship, allows the observations to be explained adequately (to first order) by the following model.

Vector magnetic field measurements onboard a ship are the sum of the ambient geomagnetic field at the vessel location and the induced and remanent magnetic fields of the ship expressed as (Isezaki 1986):

$$\mathbf{B_{obs}} = \underline{R}\,\underline{P}\,\underline{Y}\,\mathbf{B} + \underline{A}\,\underline{R}\,\underline{P}\,\underline{Y}\,\mathbf{B} + \mathbf{B_p} \qquad (4.22)$$

where $\mathbf{B_{obs}}$ is the observed magnetic field vector, $\underline{R}$, $\underline{P}$ and $\underline{Y}$ are the three matrices of rotation due to the roll, pitch and yaw, respectively (see Fig. 4.3), $\mathbf{B}$ is the ambient magnetic field vector, and $\underline{A}$ is the magnetic susceptibility tensor of the ship for a given location of the sensor. Finally, $\mathbf{B_p}$ corresponds to the remanent magnetic field vector of the ship, and $\underline{A}\mathbf{B}$ is the field vector due to the ship's induced magnetic moment. R, P, and Y are given by the attitude sensor measurements. Once $\underline{A}$ and $\mathbf{B_p}$ are known, it becomes possible to determine the ambient geomagnetic field $\mathbf{B}$ from the measurements $\mathbf{B_{obs}}$ (Isezaki 1986).

To determine $\underline{A}$ and $\mathbf{B_p}$, the usual technique is to acquire calibration data at a location where the ambient geomagnetic field $\mathbf{B}$ does not vary much and can be approximated by the IGRF field model. Specific navigation maneuvers called 'figures of eight' are carried out: they consist of a two consecutive narrow circles of opposite direction, i.e., a clockwise and a counterclockwise loops. The loops in opposite directions result in opposite ship roll, a way to sample the widest possible range of relative orientations of the ship and the ambient field. A large range of relative orientations insures a better constrained determination of $\underline{A}$ and $\mathbf{B_p}$ by least-squares inversion of the calibration loop data (Isezaki 1986; Seama et al. 1993; Korenaga 1995). A faster alternative to figures of eight for ships equipped with bow thrusters is to undertake 360° rotations. Whereas Isezaki (1986) used the IGRF models to assign a value to $\mathbf{B}$ (so with uncertainty), Lesur et al. (2004) performed their own absolute measurements during the rotation, directly estimating the field strength assuming that the bulk susceptibility of the vessel is isotropic. The latter is true for a fibreglass boat, but not for steel research vessels. The accuracy of such an approach reaches 0.2° in declination, 0.05° in inclination and 10 nT in total intensity values. The accuracy of STCM measurements is not better than several tens of nT and can be improved by filters applied to improve the signal to noise ratio (Korenaga 1995).

STCM has been widely used by Japanese research vessels for the last 20 years (Isezaki 1986; Seama et al. 1993; Korenaga 1995) and are getting more popular in Korea (Lee and Kim 2004), France and Germany (König 2006). A difficulty is that, how ever carefully the calibration loops and the reduction of the data are performed, noise still affects the data, because the model used to estimate the ship's magnetization is so simplistic. For instance, the viscous remanent magnetization acquired by a ship sailing on the same heading for a long time will result in a slow and systematic variation of the anomalies, easily removed with a linear regression. Other more complex effects involve Foucauld currents in the ship, a conductive body moving in the Earth's magnetic field. For these reasons, the STCM measurements are only relative estimates of the geomagnetic vector useful for crustal anomaly studies, whereas the proton precession and Overhauser magnetometers provide absolute values of the field amplitude suitable for geomagnetic studies. The two types of measurements are complementary.

4.16.2 Deep-Sea Magnetic Observations

Sea-surface magnetic observations, typically acquired more than 2000 m above the magnetized sources, lack sufficient resolution to address some scientific problems. Here 'resolution' does not means the resolution of the instrument but the ability of the recorded signal (the magnetic anomaly) to detect a given variation of the causative physical property (the magnetization of a source body). Sea-surface anomalies barely resolve the longest wavelengths of geomagnetic field intensity as recorded by the oceanic crust (e.g., Canda and Kent 1992a, 1992b; Gee et al. 1996; Bouligand et al. 2006). Simple forward modelling easily demonstrates that the details of these variations or the depiction of ore deposits on the seafloor in association with hydrothermal vents, for instance, are beyond the reach of these data (e.g., Tivey and Dyment 2010).

The magnetic field created by a point source decays as $\frac{1}{r^3}$, where r is the distance to the source body ($\ln(\frac{1}{r})$ in the case of a 2D problem, i.e., a line source seen as a point source in cross section). The only way to significantly improve the resolution of the magnetic signal caused by a source bodies is to reduce the distance to these bodies. For marine magnetics, this means evolving from sea-surface to deep-sea measurements.

4.16.2.1 Procedures

There are two ways to get magnetic profiles closer to the seafloor: either towing a magnetometer behind a depressing weight (deep tow magnetometer), or attaching a magnetometer to a deep-sea vessel, either a manned submersible, a Remotely Operated Vehicle (ROV) or an Autonomous Underwater Vehicle (AUV). Deep tow magnetometers are most often operated at between 200 m and 1000 m above the seafloor (depending the depth and roughness of the seafloor, the desired speed of the ship, and the confidence on the navigation), whereas deep-sea vehicles are generally used up to about 50 m above the seafloor. In both cases, the magnetometer must be placed in a pressure case adapted to the operation depth. Both require slow speeds: about 1.5–2 knots for a deep tow instrument, depending on the water depth and the altitude above seafloor of the measurements; 0.5–1 knot for deep-sea vehicles, depending on the type of vehicle and the depth of the dive, compared with the usual 10–12 knots of most oceanographic vessels. For this reason, and because of the higher level of technology required for such experiments, deep-sea magnetic measurements are expensive and sparse.

Another difficulty common to every deep-sea experiment is accurate positioning of the instrument. Unlike the sea-surface magnetometer, towed 200 to 300 m behind the ship and quite easy to locate with reasonable accuracy, the deep tow magnetometer has a cable several kilometers long. Its positioning requires either a depthmeter – to compute an estimated position assuming that the cable is not bending much and currents are not deviating the instrument laterally from the ship's profile – or a beacon emitting acoustic signals to the ship's Ultra Short BaseLine (USBL) receiver, if such a positioning system is available, or a combination of both for better results. The deep-sea vehicle is usually located by a Long BaseLine (LBL) positioning system – implying the mooring of beacons prior to the experiment – or by a USBL system as well. In both cases, the position of the ship (for USBL) and, to a lesser extent, of the beacons (location of moorings, for LBL) are well known from GPS. Detailed surveys by submersibles or ROVs rely on both acoustic positioning and dead-reckoning navigation; in addition, they also use artificial markers provisionally set up on the seafloor at the beginning of the survey and regularly revisited during the survey to avoid any drift in navigation. The accuracy of such navigation is similar to that of GPS, i.e., a few tenths of meters or better, whereas that of deep-tow magnetometers may be closer to a few hundred of meters - probably better if only relative accuracy along the profile is considered.

Deep tow magnetometers can be either autonomous, i.e., a magnetometer, a pack of batteries, and a recording device is towed at the end of a passive cable, or connected to the ship by a conducting cable which provides power to the instrument and real-time data transfer to the ship. Although the latter is far better for unlimited autonomy and real-time control of the instrument (i.e., to insure that the instrument is properly operating and to get the depth of the instrument for safer monitoring of the cable length and the ship's speed), conducting cables are rather expensive and are not readily available on all research vessels. The major difficulty in operating a deep tow magnetometer is with altitude control, and loss of instruments after collision with the seafloor is not uncommon.

Most deep tow magnetometers are scalar devices–proton precession, Overhauser, or the less accurate but cheaper, easier to operate and often adequate magnetoresistive instruments (e.g., Lenz 1990). Fluxgate magnetometers are sometime used to provide the magnetic field intensity, without any specific attempt to obtain the vector components. A deep tow vector magnetometer, quite similar in principle to the surface towed vector magnetometer described above, has been constructed and sucessfully operated on the East Pacific Rise (EPR, Yamamoto et al. 2004, 2005).

Due to its proximity to the seafloor and for safety reasons, it is impossible to tow a scalar magnetometer behind a deep-sea vessel. The magnetometer has to be attached to the hull of the vessel, at the most extreme position as possible, and should therefore be a vector magnetometer, i.e., three orthogonal fluxgate sensors. The method to correct for the magnetic effect

of the vessel is similar to the one described above for STCM. Loops which can be used for calibration are spontaneously performed by submersibles like DSS Nautile of IFREMER (because of its slightly unbalanced weight). ROVs can easily be stopped in the mid-water column, far from both the magnetic sources of the seafloor and the ship, to achieve 360° rotations using their lateral thrusters. AUVs can sail calibration loops, if their magnetic effect is large enough to require a correction.

Topography and altitude variations dominate the magnetic signal recorded by a deep-sea vessel, and have a significant effect on deep tow measurements. Modeling and filtering methods (e.g., Guspi 1987; Hussenoeder et al. 1995; Honsho et al. 2009) help to extract the signal of interest, i.e., seafloor magnetization variations.

4.16.2.2 Some Applications

Despite their cost, a significant number of deep-sea magnetic experiments have been carried out for specific societal or scientific purposes.

One of the first cruises to use a deep-tow magnetometer was undertaken to find the wreck of the sunken submarine Thresher in the Northwest Atlantic (Heirtzler 1964, and references therein). The instrument was towed at a depth of ∼3000 meters and an altitude of 20–25 m above the seafloor. Although the accuracy of their proton magnetometer TF measurements was 3 nT, they estimated the true error to be ∼10 nT considering the error on sensor position.

Many deep-sea magnetic experiments have taken place at mid-ocean ridges, as part of the effort to explore them. Klitgord et al. (1975) performed several deep tow profiles across the EPR. Macdonald et al. (1983) demonstrated the outward dipping slope of the polarity boundaries, which results from the combination of lava piling and seafloor spreading, by considering measurements at different altitudes above the EPR. This was later confirmed by direct measurements on the Blanco Fracture Zone (Tivey et al. 1998a). Gee et al. (2000) and Pouliquen et al. (2001a, b) have shown from deep tow measurements on the EPR and the Central Indian Ridge, fast and intermediate spreading center respectively, that the oceanic crust is confidently recording not only geomagnetic polarity reversals but also the geomagnetic intensity variations. Honsho et al. (2009) extended this observation to the magmatic areas of slow spreading centers from submersible observations on the Mid-Atlantic Ridge. These observations are allowing high resolution dating of the seafloor using geomagnetic intensity variations in the well-constrained Brunhes and Matuyama sequences. Tivey et al. (1998b) have been able to map the thickness of a recent lava flow from its magnetic signature as recorded by AUV ABE of WHOI on the Juan de Fuca Ridge. Conversely, Shah et al. (2003) have used the same AUV to map the ultrafast EPR at 18°S and found a magnetic low interpreted as depression as the signature of hot dykes, as well as lobes that may mark different lava flows erupted under different geomagnetic paleointensities.

Other important features that exhibit magnetic signature at deep-sea vessel altitudes are active and fossil hydrothermal sites (e.g., Tivey and Dyment 2010). Sites lying on a basaltic basement are associated with a negative magnetic anomaly, i.e., the titanomagnetites are altered to titanomaghemites and non magnetic minerals under the effect of pervasive hydrothermal fluid circulation (Tivey et al. 1993; Tivey and Johnson 2002). Conversely, sites lying on ultramafic rocks such as site Rainbow on the Mid Atlantic Ridge are associated with a strong positive anomaly (Dyment et al. 2005), possibly the result of new magnetic minerals created by serpentinization (magnetite) or by sulfide deposition and accumulation (pyrrhotite). These results suggest deep-sea magnetics is a suitable method to detect and characterize fossil hydrothermal vents and evaluate the mining potential of such ore deposits on the seafloor.

Deep-sea magnetics data have also been collected over passive margins, for instance on the peridotite ridge off Galicia (e.g. Whitmarsh and Miles 1995). Sibuet et al. (2007) used deep-tow magnetic measurements to suggest that serpentinization of outcropping mantle at some oceanic margins could generate parallel magnetic lineations similar to seafloor spreading anomalies. Another successful application is seamount magnetism, where Gee et al. (1988) mapped the non-uniform magnetization of Jasper seamount with sufficient resolution to better constrain paleomagnetic poles than would have been done with surface magnetic measurements. In general, deep-sea magnetic measurements are combined with other geological and structural information to determine an equivalent magnetization distribution (given a magnetized source

geometry), to be compared to rock magnetic property measurements (Macdonald et al. 1979; Gee et al. 1988; Ravilly et al. 2001; Honsho et al. 2009).

4.17 Conclusions for Marine Magnetics

Several aspects of marine magnetic observations have been reviewed, trying to emphasize the evolution of errors associated with such data. The scalar measurement is very large dataset and covers all northern parts of oceans very well, but which shows gaps in the southern oceans. Most of these data were acquired between 1960 and 1980. Even though early data are affected by different kind of errors (such as no correction for the external field), one can retrieve the true magnetic anomaly value by applying Comprehensive Models. Also, instrumental errors have been considerably reduced with improvements in scalar magnetometers such as Overhauser sensors. Vector measurements are becoming more common in scientific marine campaigns mainly because specific sailing techniques like 'Figures of Eight' and data processing now allow the initial problems of sensor orientation and ship noise contribution to be overcome. Finally, to map the small-wavelength magnetic anomalies over oceanic areas, deep-sea magnetic measurements have been undertaken for the last 20 years. The results of such observations have considerably improved our vision of the shallow crust's magnetization, and it is now a field of research in its own right.

4.18 General Conclusion

In this manuscript we try to give an overview of the magnetic data acquisition and processing techniques for both airborne and marine surveys. These techniques have constantly evolved since they appeared at the turn of the 20th century. Whereas a century ago researcher were trying to acquire data at "higher and higher" altitudes for the sake of complete coverage of large areas, nowadays "lower and lower" altitudes are aimed for the sake of higher resolution. Major technological improvements in instrumentation for both the acquisition of magnetic measurements and navigational data, favored higher accuracy and resolution field mapping. For aeromagnetics, this implies that the survey have to be flown at very low altitudes, whereas for marine magnetic data acquisition, measurements have to be closer to the ocean floor. The Unmanned Aerial Vehicle (UAV) and both the Autonomous Underwater Vehicle (AUV) and Remotely Operated Vehicle (ROV) are seen as solutions for acquiring safely and efficiently such data. The developments of these techniques will continue in the future as: (1) Large areas are still to be surveyed, particularly over the Oceans; (2) Significant efforts are still required to patch together the existing surveys; (3) intermediate wavelength magnetic anomalies ($\sim$500 km) are not yet properly mapped.

Acknowledgements The authors collectively would like to thank the reviewer, Kathryn Whaler, and acknowledge her work that greatly improved the quality of manuscript. MH would like to warmly acknowledge the contributions of K. Allek, N. Bournas, J. Luis in compiling and processing aeromagnetic data and P. Mouge for his help. T. Ishihara kindly accepted to review a preliminary version of the part devoted to marine magnetics. YQ also acknowledges him and M. Catalãn for precious references that helped to build and write the marine magnetics sections. Novatem, and Geometrics companies kindly provided illustrations used in this article.

References

Achache J, Cohen Y, Unal G (1991) The french program of circumterrestrial magnetic surveys using startospheric balloons. EOS Trans Am Geophys Union 72:97–101

Acuña MH, Scearce CS, Seek JB, Scheifele J (1978) The magsat vector magnetometer-a precision fluxgate magnetometer for the measurement of the geomagnetic field, Technical report, NASA/GSFC TM 79656

Acuña MH, Connerney JEP, Ness NF, Lin RP, Mitchell D, Carlson CW, McFadden J, Anderson KA, Reme H, Mazelle C, Vignes D, Wasilewski P, Cloutier P (1999) Global distribution of crustal magnetization discovered by the mars global surveyor MAG/ER experiment. Science 284(5415):790–793

Airo ML (2002) Aeromagnetic and aeroradiometric response to hydrothermal alteration. Surv Geophys 23:273–302

Allan T (1969) A review of marine geomagnetism. Earth Sci Rev 5:217–254

Allek K (2005) Traitement et interpretation des donnees aeromagnetiques acquises au-dessus des regions de tindouf et de l'eglab (SO de l'Algerie): impact sur l'exploration du diamant, Master's thesis, Universite des Sciences et de la Technologie Houari Boumediene, USTHB

Allek K, Hamoudi M (2008) Regional-scale aeromagnetic survey of the south-west of algeria: a tool for area selection for diamond exploration. J Afr Earth Sci 50:67–78

Anderson B, Longacre M, Quist P (1999) Comparison of a new marine magnetometer system to high-resolution aeromagnetic data a case study from offshore Oman. In: Proceedings of the SEG International Exposition and 70th Annual Meeting, Houston

Anderson DE, Pita AC (2005) Geophysical surveying with georanger uav. Am Inst Aeronaut Astronaut 50:67–78

Balsley JRJ (1946) The airborne magnetometer, Preliminary report 3, 8p., U.S. Geological Survey, Washington, DC

Barton CE (1997) International geomagnetic reference field: The seventh generation. J Geomagnetic Geoelectric 49: 123–148

Bell WE, Bloom AL (1957) Optical detection of magnetic resonance in alkali metal vapor. Phys Rev 107(6): 1559–1565

Bhattacharyya BK (1969) Bicubic spline interpolation as a method for treatment of potential field data. Geophysics 34:402–423

Bhattacharyya BK (1971) An automatic method of compilation and mapping of high-resolution aeromagnetic data. Geophysics 36(4):695–716

Binder AB (1998) Lunar prospector: overview. Science 281(5382):1475–1476

Blakely RJ (1988) Curie temperature isothermal analysis and tectonic implications of aeromagnetic data from Nevada. J Geophys Res 93(B10):11817–11832

Blakely R, Cox A, Iufer E (1973) Vector magnetic data for detecting short polarity intervals in marine magnetic profiles. J Geophys Res 78:6977–6983

Bouligand C, Dyment J, Gallet Y, Hulot G (2006) Geomagnetic field variations between chrons 33r and 19r (83–41 ma) from sea-surface magnetic anomaly profiles. Earth Planet Sci Lett 250(3–4):541–560. doi:10.1016/j.epsl.2006.06.051

Bournas N (2001) Interpretation des donnees aerogeophysiques acquises au-dessus du hoggar oriental (algerie), PhD thesis, Universite des Sciences et de la Technologie Houari Boumediene, USTHB

Bournas N, Galdeano A, Hamoudi M, Baker H (2003) Interpretation of the aeromagnetic map of eastern hoggar (algeria) using euler deconvolution, analytic signal and local wavenumber methods. J Afr Earth Sci 37:191–205

Boyce J, Reinhardt E, Raban A, Pozza M (2004), Marine Magnetic Survey of a Submerged Roman Harbour, Caesarea Maritima, Israel. Int J Naut Arch 33(1):122–136. doi:10.1111/j.1095-9270.2004.010.x

Bozzo E, Colla A, Caneva G, Meloni A, Caramelli A, Romeo G, Damaske D, Moeller D (1994) Technical procedures for aeromagnetic surveys in antarctica during the italian expeditions (1988–1992). Ann Geophys XXXVII(5):1283–1294

Braginski SI, Roberts PH (1995) Equations governing convection in earth's core and the geodynamo. Geophys Astrophys Fluid Dyn 79(1):1–97

Briggs IC (1974) Machine contouring using minimum curvature. Geophysics 39:39–48

Bullard E, Mason R (1961) The magnetic field astern of a ship. Deep Sea Res 8:20–27

Cady JW (1990) Alaska as a frontier for aeromagnetic interpretation. In: Geologic applications of modern aeromagnetic surveys. U.S. Geological Survey Bulletin 1924:75–84

Cande S, Kent D (1992a) A new geomagnetic polarity time scale for the late Cretaceous and Cenozoic. J Geophys Res 97:13917–13951

Cande S, Kent D (1992b) Ultrahigh resolution marine magnetic anomaly profiles: a record of continuous paleointensity variations. J Geophys Res 97:15075–15083

Chapman S, Bartels J (1940) Geomagnetism, vol. II. Clarendon Press, Oxford, p 633

Chiappini M, Meloni A, Boschi E, Faggioni O, Beverini N, Carmiciani C, Marson I (2000) Shaded relief magnetic anomaly map of italy and surrounding marine areas. Ann Geophys 43(5):983–989

Cohen TJ, Lintz PR (1974) Long term periodicities in the sunspot cycle. Nature 250:398–399

Cohen Y, Menvielle M, Le Mouël J (1986) Magnetic measurements aboard a stratospheric balloon. Phys Earth Planetary Inter 44:348–357

Cordell LE, Hildenbrand TG, Kleinkopf MD (1990) Notes of discussion group on the midcontinent. In: Geologic applications of modern aeromagnetic surveys. U.S. Geological Survey Bulletin 1924:90–91

Courtillot V, Le Mouël J, Mayaud P (1977) Maximum entropy spectral analysis of the geomagnetic activity index aa over 107-year interval. J Geophys Res 82(19):2641–2649

Dehmelt HG (1957) Slow spin relaxation of optically polarized sodium atoms. Phys Rev 105(5):1487–1489

Dobrin MD, Savit CH (1988) Introduction to geophysical prospecting. Mc Graw Hill, New York, NY, p 867

Doll WE, Gamey TJ, Beard LP, Bell DT (2006) Airborne vertical magnetic gradient for near-surface applications. The Leading Edges 25(1):50–53

Doyle HA (1987) Geophysics in Australia. Earth Sci Hist 6(2):178–204

Dyment J, Tamaki K, Horen H, Fouquet Y, Nakase K, Yamamoto M, Ravilly M, Kitazawa M (2005) A positive magnetic anomaly at Rainbow hydrothermal site in ultramafic environment. Eos Trans AGU 86(52, Fall Meet Suppl): 21–08

Engels M, Barckhausen U, Gee J (2008) A new towed marine vector magnetometer: methods and results from a Central Pacific cruise. Geophys J Int 172:115–129. doi:10.1111/j.1365-246X.2007.03601.x

Eve AS (1932) A magnetic method for estimating the height of some buried magnetic bodies. Trans Geophys Prospect Am Inst Mining Metallurgical Eng 101:200–215

Eve AS, Keys DA (1933) Applied geophysics in the search for minerals. Cambridge University Press, Cambridge

Ferris JK, Vaughan APM, King EC (2002) A window on west Antarctic crustal boundaries: the junction between the antarctic peninsula, the filchner block and weddell sea oceanic lithosphere. Tectonophysics 347:13–23

Finlay C, Maus S, Beggan C, Hamoudi M, Lowes FJ, Olsen N, Thèbault E (2010) Evaluation of candidate geomagnetic field models for igrf-11. Earth Planets Space submitted 1–18

Foster MR, Jines WR, van der Weg K (1970) Statistical estimation of syetematic errors at intersections of lines of aeromagnetic survey data. J Geophys Res 75:1507–1511

Frost BR, Shive PN (1986) Magnetic mineralogy of the lower continental crust. J Geophys Res 91(B6):6513–6521

Gee J, Schneider D, Kent D (1996) Marine magnetic anomalies as recorders of geomagnetic intensity variations. Earth Planet Sci Lett 144:327–335

Gee J, Tauxe L, Hildebrand J, Staudigel H, Lonsdale P (1988) Nonuniform Magnetization of Jasper Seamount. J Geophys Res 93(B10):12159–12175

Gee J, Cande S (2002) A surface-towed vector magnetometer. Geophys Res Lett. doi:10.1029/2002GL015245

Gee J, Cande S, Hildebrand J, Donnelly K, Parker R (2000) Geomagnetic intensity variations over the past 780 kyr obtained from near-seaoor magnetic anomalies. Nature 408:827–832

Germain-Jones D (1957) Post-war developments in geophysical instrumentation for oil prospecting. J Sci Inst 34:1–8

Gopal BJ, Sarma VN, Rambabu HV (2008) Real time compensation for aircraft induced noise during high resolution airborne magnetic surveys. J Ind Geophys Union 8(3):185–189

Grant F (1970) Statistical models for interpreting aeromagnetic data. Geoexploration 35(2):293–302

Grant F (1972) Review of data processing and interpretation methods in gravity and magnetics, 1964–71. Geophysics 37(2):647–661

Grant F (1985a) Aeromagnetics, geology, and ore environments; i, magnetite in igneous, sedimentary and metamorphic rocks—an overview. Geoexploration 23:303–333

Grant F (1985b) Aeromagnetics, geology and ore environments; ii, magnetite and ore environments. Geoexploration 23: 335–362

Grauch VJS, Millegan P (1998) Mapping intrabasinal faults from high-resolution aeromagnetic data. The Leading Edges 17(1):53–56

Guspi F (1987) Frequency-domain reduction of potential field measurements to a horizontal plane. Geoexploration 24: 87–98

Hamoudi M, Cohen Y, Achache J (1998) Can the thermal thickness of the continental lithosphere be estimated from magsat data. Tectonophysics 284:19–29

Hamoudi M, Thèbault E, Lesur V, Mandea M (2007) Geoforschungszentrum anomaly magnetic map (gamma): a candidate model for the world digital magnetic anomaly map. Geochem Geophys Geosyst 8(6):1–13

Hanna WF (1990) Some historical notes on early magnetic surveying in the U.S. geological survey. In: Geologic applications of modern aeromagnetic surveys. U.S. Geological Survey Bulletin 1924:63–73

Hansen RO (1993) Interpretive gridding by anistropic kriging. Geophysics 58(10):1491–1497

Hardwick CD (1984a) Important design considerations for inboard airborne magnetic gradiometers. Geophysics 49(11):2004–2018

Hardwick CD (1984b) Non-oriented cesium sensors for airborne magnetometry and gradiometry. Geophysics 49(11): 2024–2031

Hawkins WB (1955) Orientation and alignment of sodium atoms by means of polarized resonance radiation. Phys Rev 98(2):478–486

Heezen B, Ewing M, Miller E (1953) Trans-Atlantic profile of total magnetic intensity and topography, Dakar to Barbados. Deep Sea Res 1:25–33

Heiland CA (1929) Geophysical methods of prospecting: Principles and recent successes. Q Colo School Mines XXIV(1):47–77

Heiland CA (1935) Geophysical mapping from the air: its possibilities and advantages. Eng Min J 136: 609–610

Heiland CA (1940) Geophysical exploration. Prentice-Hall, New York, NY

Heiland CA (1953) Method of and apparatus for aeromagnetic prospecting U.S. Patent 2659859

Heirtzler J (1964) Magnetic measurements near the deep ocean floor. Deep Sea Res 11:891–898

Hemant K, Thèbault E, Mandea M, Ravat D, Maus S (2007) Magnetic anomaly map of the world: merging satellite, airborne, marine and ground-based magnetic data sets. Earth Planetary Sci Lett 260(1–2):56–71

Hildenbrand TG, Raines GL (1990) Need for aeromagnetic data and a national airborne geophysics program. In: Geologic applications of modern aeromagnetic surveys. U.S. Geological Survey Bulletin 1924:1–5

Hill M (1959) A ship-borne nuclear-spin magnetometer. Deep Sea Res 5:309–311

Hofman-Wellenhof B, Legat K, Wiener M (2003) Navigation: principles of positioning and guidance. Springer, New York, NY

Honsho C, Dyment J, Tamaki K, Ravilly M, Horen H, Gente P (2009) Magnetic structure of a slow spreading ridge segment: insights from near-bottom magnetic measurements on board a submersible. J Geophys Res. 114 B05101:1–25 doi:10.1029/2008JB005915

Hood L, Zakharian A, Halekas J, Mitchell D, Lin R, na MA, Binder A (2001) Initial mapping and interpretation of lunar crustal magnetic anomalies using lunar prospector magnetometer data. J Geophys Res 106(E11):27825–27839

Hood P (1990) Aeromagnetic survey program of Canada, mineral applications, and vertical gradiometry, in Geologic Applications of Modern Aeromagnetic Surveys

Hood P (2007) History of aeromagnetic surveying in Canada. The Leading Edges 26(11):1384–1392

Hood P, Sawatzky JP, Kornik LJ, McGrath PH (1976) Aeromagnetic gradiometer survey, white lake, Open File 339, Geological Survey of Canada

Horsfall KR (1997) Airborne magnetic and gamma-ray acquisition. J Aust Geol Geophys 17(2):23–30

Hrvoic D (2007) SeaSPY technical application guide, marine magnetics corporation education

Hussenoeder SA, Tivey MA, Schouten H (1995) Direct inversion of potential fields from an uneven track with application to the Mid-Atlantic Ridge. Geophys Res Lett 22:3131–3134. doi:10.1029/95GL03326

Isezaki N (1986) A new shipboard three-component magnetometer. Geophysics 51(10):1992–1998

Jensen H (1965) Instrument details and applications of a new airborne magnetometer. Geophysics XXX(5): 875–882

Jones E (1999) The earth's magnetic field at sea, in marine geophysics. Wiley, Chichester, pp 162–197

Kastler A (1954) Optical methods of atomic orientation and of magnetic resonance. J Opt Soc Am 47(6):460–465

Keating P (1993) The fractal dimension of gravity data sets and its implication for gridding. Geophys Prospect 41: 983–994

Keating P (1995) A simple technique to identify magnetic anomalies due to kimberlite pipes. Explor Mining Geol 4:121–125

Kittel C (2005) Introduction to the solid state physics. Wiley, San Francisco, CA

Klitgord K, Mudie J, Huestis S, Parker R (1975) An analysis of near-bottom magnetic anomalies: sea-floor spreading

and the magnetized layer. Geophys. J R Astron Soc 43: 387–424
König M (2006) Processing of shipborne magnetometer data and revision of the timing and geometry of the Mesozoic breakup of Gondwana. Rep Polar Res 525:137 pp.
Korenaga J (1995) Comprehensive analysis of marine magnetic vector anomalies. J Geophys Res 100(B1):365–378
Korhonen JV (2005) Airborne magnetic method: Special features and review on applications, In: Airo ML (ed) Aerogeophysics in Finland 19722004: methods, system characteristics and applications, vol 39. Geological Survey of Finland, special paper Espoo, Finland edn. pp 77–102
Korhonen JV, Koistinen T, Elo S, Saavuori H, Kaariainen J, Nevanlinna H, Aaro S, Haller LA, Skilbrei JR, Solheim D, Chepik A, Kulinich A, Zhdanova L, Vaher R, All T, Sildvee H (1999) Preliminary magnetic and gravity anomaly maps of the fennoscandian shield 1:10, 000, 000. Geological Survey of Finland 27 Special paper, pp 173–179
Korhonen J, Fairhead J, Hamoudi M, Hemant K, Lesur V, Mandea M, Maus S, Purucker M, Ravat D, Sazonova T, Thèbault E (2007) Magnetic anomaly map of the World, Scale 1:50,000,000, 1st edn. Commission for the Geological Map of the World, UNESCO edn.
Langel R (1982) The magnetic earth as seen from magsat, initial results. Geophys Res Lett 9(4):239–242
Langel R, Ousley G, Berbert J, Murphy J, Settle M (1982) The magsat mission. Geophys Res Lett 9(4):243–245
Langel R, Hinze W (1998) The magnetic field of the Earth's lithosphere. Cambridge University Press, Cambridge
Laughton A, Hill M, Allan T (1960) Geophysical investigations of a Seamount 150 miles North of Madeira. Deep Sea Res 7:117–141
Le Mouël JL (1969) Les elements du champ magnetique terrestre, PhD thesis, Faculte des Sciences de l'Universite de Paris
Lee S, Kim S (2004) Vector magnetic analysis within the southern Ayu Trough, equatorial western Pacific. Geophys J Int 156:213–221
Leger JM, Bertrand F, Jager T, Prado ML, Fratter I, Lalaurie JC (2009) Swarm absolute scalar and vector magnetometer based on helium 4 optical pumping. Procedia Chem 1: 634–637
Leliak P (1961) Identification and evaluation of magnetic field sources of magnetic airborne detector equiped aircraft. Ins Radio Eng Trans Aerospace Navigational Electron 8: 95–105
Lenz J (1990) A review of magnetic sensors. Proc IEEE 78(6):973–989
Lesur V, Clark T, Turbitt C, Flower S (2004) A technique for estimating the absolute vector geomagnetic field from a marine vessel. J Geophys Eng 1:109–115
Lesur V, Wardinski I, Rother M, Mandea M (2008) GRIMM: the GFZ reference internal magnetic model based on vector satellite and observatory data. Geophys J Int 173(2): 382–394. doi:10.1111/j.1365-246X.2008.03724.x
Lesur V, Wardinski I, Asari S, Minchev B, Mandea M (2009) Modelling the Earth's core magnetic field under flow constraints. Earth Planet Space 62(6):503–516
Logachev AA (1947) The development and applications of airborne magnetometers in the u.s.s.r. Geophysics (trans: Russian Hawkes HE) 11:135–147
Luis JF (1996) Le leve aeromagnetic des acores, PhD thesis, Institut de Physique du Globe de Paris, IPGP
Luis JF, Miranda JM (2008) Reevaluation of magnetic chrons in the north atlantic between 35n and 47n: Implications for the formation of the azores triple junction and associated plateau. J Geophys Res 113(B10105):1–12
Luis JF, Miranda JM, Galdeano A, Patriat P, Rossignol JC, Mendes-Victor LA (1994) The acores triple junction evolution since 10 ma from aeromagnetic survey of the mid-atlantic ridge. Earth Planetary Sci Lett 125: 439–459
Lum CW (2009) Coordinated searching and target identification using teams of autonomous agents, PhD thesis, University of Washington
Lum CW, Rysdyk RT, Pongwunwattana A (2005) Autonomous airborne geomagnetic surveying and target identification, in AIAA Infotech@Aerospace Conference
Macdonald K, Kastens K, Spiess F, Miller S (1979) Deep tow studies of the Tamayo Transform Fault. Marine Geophys Res 4:37–70
Macdonald K, Miller S, Luyendyk B, Atwater T, Shure L (1983) Investigation of a Vine-Matthews magnetic lineation from a submersible: the source and character of marine magnetic anomalies. J Geophys Res 88:3403–3418
Macmillan S, Maus S (2005) International Geomagnetic Reference Field-the tenth generation. Earth Planets Space 57:1135–1140
Macmillan S, Maus S, Bondar T, Chambodut A, Golovkov V, Holme R, Langlais B, Lesur V, Lowes F, Luhr H, Mai W, Mandea M, Olsen N, Rother M, Sabaka TJ, Thomson A, Wardinski I (2003) The ninth-generation international geomagnetic reference field. Phys Earth Planetary Inter 140:253–254
Malahoff A, Feden R, Fleming H (1982) Magnetic Anomalies and Tectonic Fabric of Marginal Basins North of New Zealand. J Geophys Res 87(B5):4109–4125
Mason R (1958) A magnetic survey off the west coast of the United States between latitudes 32° and 36°N, longitudes 121° and 128°W. Geophys J 1:320–329
Mason R, Raff A (1961) A magnetic survey off the west coast of North America, 32°N to 42°N. Geol Soc Am Bull 72: 1259–1265
Maus S, McLean S, Dater D, Luhr H, Rother M, Mai W, Choi S (2005) Ngdc/gfz candidate models for the 10th generation internationale geomagnetic reference field. Earth Planets Space 57:1151–1156
Maus S, Sazonova T, Hemant K, Fairhead JD, Ravat D (2007) National geophysical data center candidate for the world digital magnetic anomaly map. Geochem Geophys Geosyst 8(6):10
Maus S, Macmillan S, McLean S, Hamilton B, Thomson A, Nair M (2009) The us/uk world magnetic model for 2010–2015, Technical Report NES-DIS/NGDC, NOAA
McCafferty AE, Van Gosen BS (2009) Airborne gamma-ray and magnetic anomaly signatures of serpentinite in relation to soil geochemistry. Appl Geochem 24: 1524–1537
Merkouriev S, DeMets C (2006) Constraints on Indian plate motion since 20 ma from dense Russian magnetic data: Implications for Indian plate dynamics. Geochem Geophys Geosyst Q02002. doi:10.1029/2005GC001079

Merkouriev S, DeMets C (2008) A high-resolution model for EurasiaNorth America plate kinematics since 20 ma. Geophys J Int. doi:10.1111/j.1365-246X.2008.03761.x
Merrill R, McElhinny M (1983) The earth's magnetic field: its history, origin, and planetary perspective. Academic, London
Miles PJ, Partner RT, Keeler KR, McConnel TJ (2008) Unmanned airborne vehicle geophysical surveying US 2008/0125920 A1
Millegan P (2005) Broader spectrum, fewew folks-gavity and magnetics. The Leading Edges 24(S1):36–41
Milligan PR, Franklin R (2004) Magnetic anomaly map of Australia, 4th edn. Geoscience Australia, Canberra, Scale 1:5,000,000
Milligan PR, White A, Heinson G, Brodie R (1993) Micropulsation and induction array study near ballarat victoria. Explor Geophys 24(2):117–122
Minty BRS (1991) Simple micro-levelling for aeromagnetic data. Explor Geophys 22:591–592
Mittal PK (1984) Algorithm for error adjustment of potential field data along a survey network. Geophysics 49(4):467–469
Muffly G (1946) The airborne magnetometer. Geophysics 11:321–334
Nabighian M, Grauch V, Hansen R, LaFehr T, Li Y, Peirce J, Phillips J, Ruder M (2005) The historical development of the magnetic method in exploration. Geophysics 70(6):33–61. doi:10.1190/1.2133784
Nazarova K, Tsetkov YA, Heirtzler J, Sabaka TJ (2005) Balloon geomagnetic survey at stratospheric altitudes, In: Reigber C, Luhr H, Schwintzer P, Wickert J (eds) Earth magnetic field. Springer, New York, NY, pp 273–278
Ness NF (1971) Interaction of the solar wind with the moon. Phys Earth Planetary Inter 4:197–198
Nielsen OV, Petersen JR, Primdahl F, Brauer P, Hernando B, Fernandez A, Merayo JMG, Ripka P (1995) Development, construction and analysis of the 'oersted' fluxgate magnetometer. Meas Sci Technol 6:1099–1115
Nielsen OV, Brauer P, Primdahl F, Risbo T, Jorgensen JL, Boe C, Deyerler M, Bauereisen S (1997) A high-precision triaxial fluxgate sensor for spece applications: layout and choice of materials. Sens Actuators A59:168–176
O'Connell MD, Smith RS, Vallee MA (2005) Gridding aeromagnetic data using longitudinal and transverse gradients with the minimum curvature operator. The Leading Edges 24:142–145
Olsen N (2002) A model of the geomagnetic field and its secular variation for epoch 2000 estimated from Oersted data. Geophys J Int 149:454–462
Olsen N, Lühr H, Sabaka TJ, Mandea M, Rother M, Toffner-Calusen L, Choi S (2006) CHAOS—a model of the Earth's magnetic field derived from CHAMP, Oersted, and SAC-C magnetic satellite data. Geophys J Int 166:67–75
Olsen N, Mandea M, Sabaka TJ, Toffner-Clausen L (2009) Chaos-2 —a geomagnetic field model derived from one decade of continuous satellite data. Geophys J Int 179: 1477–1487
Overhauser AW (1953) Polarization of nuclei in metals. Phys Rev 92:411–415
Packard M, Varian R (1954) Proton gyromagnetic ratio. Phys Rev 93:941–947
Pang X, Lintz C (2009) Study on aircraft magnetic compensation based on fir model, In: International Symposium on Intelligent Information Systems and Applications IISA'09 Quindao, China
Pariso J, Rommevaux C, Sempere JC (1996) Three-Dimensional Inversion of Marine Magnetic Anomalies: Implications for Crustal Accretion along the Mid-Atlantic Ridge (28°–31°30′N). Mar Geophys Res 18:85–101
Parker RL, Huestis S (1974) The Inversion of Magnetic Anomalies in the Presence of Topography. J Geophys Res 79(11):1587–1593
Parkinson BW, Enge PE (1996) Differential gps, In: Zarchan P, Parkinson B, Spilker J Jr, Axelrad P, Enge P (eds) Chapter 1, American Institute of Aeronautics and Astronautics., pp 3–49.
Parsons LW, Wiatr ZM (1962) Rubidium vapour magnetometer. J Sci Instrum 39:292–300
Paterson NR, Reeves CV (1985) Applications of gravity and magnetic surveys: The state-of-the-art in 1985. Geophysics 50(12):2558–2594
Pouliquen G, Gallet Y, Dyment J, Patriat P, Tamura C (2001a) A geomagnetic record over the last 3.5 million years from deep-tow magnetic anomaly profiles across the Central Indian Ridge. J Geophys Res 106:10941–10960
Pouliquen G, Gallet Y, Dyment J, Patriat P, Tamura C (2001b) Correction to A geomagnetic record over the last 3.5 million years from deep-tow magnetic anomaly profiles across the Central Indian Ridge. J Geophys Res 106:30549
Pulz E, Jackel KH, Linthe HJ (1999) A new optically pumped tandem magnetometer: principles and experiences. Meas Sci Technol 10:1025–1031
Purucker M, Whaler K (2007) Crustal magnetism. In: Schubert G (ed) Treatise of geophysics, vol 5. Chapter 6, Elsevier, Amsterdam:195–237
Quesnel Y, Catalán M, Ishihara T (2009) A new global marine magnetic anomaly data set. J Geophys Res B04106. doi:10.1029/2008JB006144
Raff A, Mason R (1961) A magnetic survey off the west coast of North America, 40°N to 52.5°N. Geol Soc Am Bull 72:1259–1265
Ravat D, Hildebrand T, Roest W (2003) New way of processing near-surface magnetic data: the utility of the comprehensive model of the magnetic field. Leading Edge 22: 784–785
Ravilly M, Horen H, Perrin M, Dyment J, Gente P, Guillou H (2001) NRM intensity of altered oceanic basalts: a record of geomagnetic paleointensity variations? Geophys J Int 145:401–422
Reeves CV (1993) Limitations imposed by geomagnetic variations on high quality aeromagnetic surveys. Explor Geophys 24:115–116
Reeves CV (2005) Aeromagnetic surveys: principles, practice and interpretation. e-book published by Geosoft
Reford MS (1980) Magnetic method. Geophysics 45(11): 1640–1658
Reford MS (2006) Gradient enhancement of the total magnetic field. Leading Edge 25(1):59–66
Reford MS, Sumner JS (1964) Aeromagnetics. Geophysics XXIX (4):482–516
Reid AB (1980) Aeromagnetic survey design. Geophysics 45(5):973–976
Reigber C, Luhr H, Schwintzer P (2002) Champ mission status. Adv Space Res 30(2):129–134

Reigber C, Schwintzer P, Luhr H (1999) The champ geopotential mission. Bolletino di Geofisica Terica e Applicata 40: 285–289

Reynolds RJ, Schlinger CM (1990) Notes of discussion Group on Rock Magnetics. In: Geologic applications of modern aeromagnetic surveys. U.S. Geological Survey Bulletin 1924:99–101

Reynolds RL, Rosenbaum JG, Hudson MR, Fishman NS (1990) Rock magnetism, the distribution of magnetic minerals in the earth's crust , and aeromagnetic anomalies. In: Geologic applications of modern aeromagnetic surveys

Rice JAJ (1993) Automatic compensator for an airborne magnetic anomaly detector U.S. Patent 5182514

Ridsdill-Smith TA, Dentith MC (1999) The wavelet transform in aeromagnetic processing. Geophysics 64:1003–1013

Rigoti A, Padilha AL, Chamalaun FH, Trived NB (2000) Effects of the equatorial electrojet on aeromagnetic data acquisition. Geophysics 65(2):553–558

Ripka P (1996) Noise and stability of magnetic sensors. J Magnet Magnetic Mater 157–158:424–427

Sabaka TJ, Olsen N, Langel R (2002) A comprehensive model of the quiet-time, near-earth magnetic field: Phase 3. Geophys J Int 151(1):32–68

Sabaka TJ, Olsen N, Purucker ME (2004) Extending comprehensive models of the Earth's magnetic field with Oersted and CHAMP data. Geophys J Int 159:521–547

Sapunov V, Denisov A, Denisova O, Saveliev D (2001) Proton and Overhauser magnetometers metrology. Control Geophys Geodesy 31(1):119

Schouten H, Denham C (1979) Modelling the oceanic magnetic source layer, In: Talwani M, Harrison C, Hayes D (eds) Deep drilling results in the Atlantic Ocean: ocean crust, American Geophysics Union, series 2 Washington, DC:151–159

Seama N, Nogi Y, Isezaki N (1993) A new method for precise determination of the position and strike of magnetic boundaries using vector data of the geomagnetic anomaly field. Geophys J Int 113:155–164

Sexton JL, Hinze WJ, R.B. von Frese, Braile LW (1982) Long-wavelength aeromagnetic anomaly map of the conterminous united states. Geology 10:364–369

Shah A, Cormier M, Ryan W, Jin W, Sinton J, Bergmanis E, Carlut J, Bradley A, Yoerger D (2003) Episodic dike swarms inferred from near-bottom magnetic anomaly maps at the southern East Pacific Rise. J Geophys Res 2097. doi:10.1029/2001JB000564

Sibuet J, Srivastava S, Manatschal G (2007) Exhumed mantle-forming transitional crust in the Newfoundland-Iberia rift and associated magnetic anomalies. J Geophys Res. 112 B06105 doi:10.1029/2005JB003856

Sichler B, Hékinian R (2002) Three-dimensional inversion of marine magnetic anomalies on the equatorial Atlantic Ridge (St. Paul Fracture Zone): Delayed magnetization in a magmatically starved spreading center? J Geophys Res. 107(B12):2347 doi:10.1029/2001JB000401

Slack H, Lynch V, Langan L (1967) The geomagnetic gradiometer. Geophysics 32:877–892

Smith K (1997) Cesium optically pumped magnetometers : Basic theory of operation, Technical Report M-TR91, GEOMETRICS

Stolz R, Zasarenko V, Schulz M, Chwalla A, Fritzsch L, Meyer HG, Kostlin EO (2006) Magnetic full-tensor squid gradiometer system for geophysical applications. The Leading Edges 25(2):178–180

Sundberg K, Lundberg H (1932) Magnetism. Trans Am Inst Mining Metallurgical Eng

Supper R, De Ritis R, Motschka K, Chiappini M (2004) Aeromagnetic anomaly images of volcano and southern lipari islands (aeolian archipelago, italy). Ann Geophys 47(6):1803–1810

Talwani M, Dorman J, Worzel J, Bryan G (1966) Navigation at sea by satellite. J Geophys Res 71:5891–5902

Tarlowski C, Simonis F, Whitaker A, Milligan R (1992) The magnetic anomaly map of australia. Explor Geophys 23(2):339–342

Tarlowski C, Mc Ewin AJ, Reeves CV, Barton CE (1996) Dewarping the composite aeromagnetic anomaly map of australia using control traverses and base stations. Geophysics 61(3):696–705

Telford WM, Geldart LP, Sheriff RE (1990) Applied geophysics, 2nd edn. Cambridge University Press, Cambridge

Tivey M, Dyment J (2010) The magnetic signature of hydrothermal systems in slow spreading environments, In: Rona P, Devey C, Dyment J, Murton B (eds) Diversity of hydrothermal systems on slow spreading ocean ridges, Am Geophys Union Monogr, Series 188 Washington, ISBN 978-0-87390-470-8

Tivey M, Johnson H (2002) Crustal magnetization reveals subsurface structure of Juan de Fuca Ridge hydrothermal vent fields. Geology 30:979–982

Tivey M, Rona P, Schouten H (1993) Reduced crustal magnetization beneath the active sulfide mound, TAG Hydrothermal Field, Mid-Atlantic Ridge 26°N. Earth Planet Sci Lett 115:101–116

Tivey M, Johnson H, Fleutelot C, Hussenoeder S, Lawrence R, Waters C, Wooding B (1998a) Direct measurement of magnetic reversal polarity boundaries in a cross-section of oceanic crust. Geophys Res Lett 25:3631–3634 (1998a)

Tivey M, Johnson H, Bradley A, Yoerger D (1998b) Thickness measurements of submarine lava ows determined from near-bottom magnetic field mapping by autonomous underwater vehicle. Geophys Res Lett 25:805–808

Tohyama F, Nishio Y, Yamagishi H, Yamagami T (2007) Geomagnetic field observation using fluxgate magnetometer system onboard balloons in antarctica. Proc Schl Eng Tokai Univ., Ser. E 32:19–25

Tsetkov YA, Belkin VA, Kanonidi KD, Kharitonov AL (1995) Physico-geological interpretation of the anomalous geomagnetic field measured in the stratosphere. Phys Solid Earth (English Translation) 31(4):329–332

Urquhart W (2003) Airborne magnetic surveys: Past, present and future, Canadian Exploration Geophysics Society (KEGS).

Vacquier V, Raff A, Warren R (1961) Horizontal displacements in the oor of the northeastern Pacific Ocean. Geol Soc Am Bull 72:1251–1258

Vacquier VV (1946) Apparatus for responding to magnetic field U.S. Patent 2406870

Van Den Bossche P, Coles S, Murrell D, Madotyeni Z (2004) Maritime wreck surveys: Search for the wreck of the Dutch East India Company slave ship, MEERMIN, wrecked in 1766 in Struisbaai, South Africa, Technical Report 0182, Council for Geoscience and Iziko Museums, Project 0463

Verhoef J, Roest W, Macnab R, Arkani-Hamed J (1996) Members of the Project Team, Magnetic anomalies of the Arctic and North Atlantic Oceans and adjacent land areas, Technical Report GSC Open File 3125, parts a and b (CD-ROM and project Report), Geological Survey of Canada, Dartmouth, Nova Scotia, 225pp

Vine F, Matthews D (1963) Magnetic anomalies over oceanic ridges. Nature 4897:947–949

Waters G, Phillips G (1956) A new method of measuring the Earth's magnetic field. Geophys Prosp 4:1–9

Whitham K, Loomer EI (1957) Irregular magnetic activity in northern Canada with special reference to aeromagnetic survey problems. Geophysics 22:646–659

Whitham K, Niblett ER (1961) The diurnal problem in aeromagnetic surveying in Canada. Geophysics XXVI(2): 211–228

Whitmarsh R, Miles P (1995) Models of the development of the West Iberia rifted continental margin at 40°30′N deduced from surface and deep-tow magnetic anomalies. J Geophys Res 100(B3):3789–3806

Williams PM (1993) Aeromagnetic compensation using neural networks. Neural Comput Appl 1:207–214

Wyckoff RD (1948) The gulf airborne magnetometer. Geophysics 13:182–208

Yamamoto M, Seama N, Isezaki N (2004) Genetic Algorithm inversion of geomagnetic vector data using a 2.5-dimensional magnetic structure model. Earth Planets Space 56:217–227

Yamamoto M, Seama N, Isezaki N (2005) Geomagnetic paleointensity over 1.2 Ma from deep-tow vector magnetic data across the East Pacific Rise. Earth Planets Space 57: 465–470

Zhana YX (1994) Aeromagnetic anomalies and perspective oil traps in china. Geophysics 59(10):1492–1499

Zimmerman JE, Campbell WH (1975) Tests of cryogenic squid for geomagnetic field measurements. Geophysics 40(2): 269–264

Zonenshain LP, Verhoef J, Macnab R, Meyers H (1991) Magnetic imprints of continental accretion in the ussr and adjacent areas. EOS Trans Am Geophys Union 72(29): 305–310